Chemical Engineering Journal 497 (2024) 154280

Contents lists available at ScienceDirect

Chemical Engineering Journal

journal homepage: www.elsevier.com/locate/cej

Self-condensation for enhancing the hydrophilicity of covalent organic polymers and photocatalytic hydrogen generation with unprecedented apparent quantum yield up to 500 nm

Islam M.A. Mekhemer [a,b], Ahmed M. Elewa [a], Mohamed M. Elsenety [a,c], Maha Mohamed Samy [b,d], Mohamed Gamal Mohamed [b,d], Ahmed Fouad Musa [a], Tse-Fu Huang [a], Tzu-Chien Wei [a], Shiao-Wei Kuo [d], Bo-Han Chen [e], Shang-Da Yang [e,f], Ho-Hsiu Chou [a,e,g,*]

[a] Department of Chemical Engineering, National Tsing Hua University, Hsinchu 300044, Taiwan
[b] Chemistry Department, Faculty of Science, Assiut University, Assiut 71515, Egypt
[c] Chemistry Department, Faculty of Science, Al-Azhar University, Cairo 11884, Egypt
[d] Department of Materials and Optoelectronic Science, Center of Crystal Research, National Sun Yat-Sen University, Kaohsiung 804, Taiwan
[e] Institute of Photonics Technologies, National Tsing Hua University, Hsinchu, 300044 Taiwan
[f] College of Semiconductor Research, National Tsing Hua University, Hsinchu 300044, Taiwan
[g] Photonics Research Center, National Tsing Hua University, Hsinchu 300044, Taiwan

ARTICLE INFO

Keywords:
Green Synthetic Approach
Benzoin-based COPs
B-PyTT-COP (D-π-A)
Unprecedented AQY
Photocatalytic hydrogen generation

ABSTRACT

So far, achieving high apparent quantum yield (AQY) in polymeric photocatalysts at wavelengths up to 500 nm has never been achieved. Covalent organic polymers (COPs) have the advantage of high structure function tunability. However, despite decades of development, COPs still lag in achieving high AQY value, highlighting the need for an optimal COP structural design for efficient photocatalysis. Herein, we present a green synthetic approach to synthesize five hydrophilic and non-conjugated linkage with D-π-A system benzoin-based COPs by self-condensation of multiformly monomers. Charge kinetic carrier and femtosecond transient absorption (fs-TAS) demonstrate the efficient charge transport of benzoin-based COPs. Among the synthesized photocatalysts, B-PyTT-COP (D-π-A) outperforms the COP family, with an excellent HER of 233.81 μmol h^{-1} (77935 μmol $g^{-1}h^{-1}$) using Platinum as co-catalyst. Remarkedly, B-PyTT-COP has achieved an exceptional ability to generate a high AQY value at 500 nm (65.35 %), surpassing all other materials examined thus far.

1. Introduction

Escalating environmental pollution and energy crises demand the development of clean and sustainable energy sources. Photocatalytic hydrogen evolution emerges as a promising strategy in this pursuit [1–9]. However, achieving a high apparent quantum yield (AQY) remains a formidable challenge, especially at wavelengths up to 500 nm [10]. Organic polymer semiconductors, with their tailorable optoelectronic properties, offer a potential game-changer [11–17]. Despite this tunability, reported polymeric materials often exhibit low AQY due to suboptimal structural designs [18–20]. Covalent organic polymers (COPs) offer a promising platform for photocatalytic hydrogen evolution rate (HER) due to their light element composition, strong covalent bonds, and permanent pores ranging from 1 to 100 nm [21–28]. These highly versatile materials find applications in gas capture, water treatment, catalysis, and storage, separation technologies, nano-filtration membranes, and drug delivery [25,26,29–36]. However, traditional COP designs often lack optimal integration of hydrophilic groups, light-harvesting units, and controlling their molecular-level structure, hindering their ability to efficiently convert protons to hydrogen (low HER) and achieve high AQY at wavelengths up to 500 nm [21,37–39].

Recent breakthroughs underscore the potential of covalent organic polymers (COPs) for efficient solar-to-hydrogen conversion. Xiang et al. achieved HER of 2500 μmol $g^{-1}h^{-1}$ with a COP-carbon encapsulated Ni_2P composite (COP-TF@CNi_2P), demonstrating AQY values of 2.5 and 1.5 at 400 and 500 nm, respectively [38]. Similarly, COP-$TP_{1:3}$ exhibited

* Corresponding author at: Department of Chemical Engineering, National Tsing Hua University, Hsinchu 300044, Taiwan.
E-mail address: hhchou@mx.nthu.edu.tw (H.-H. Chou).

https://doi.org/10.1016/j.cej.2024.154280
Received 20 May 2024; Received in revised form 17 July 2024; Accepted 23 July 2024
Available online 25 July 2024

an HER of 4200 μmol $g^{-1}h^{-1}$ with corresponding AQY of 1.5 and 0.5 at these wavelengths [39]. Our group further contributed by synthesizing triptycene-based COPs, where DPBT-TP COP displayed a record-breaking HER of 17806 μmol $g^{-1}h^{-1}$ and an AQY of 3.28 at 420 nm [26]. Moreover, highlighting the synergy between COPs and metal complexes, Yang et al. reported a significant HER enhancement for their bipyridyl-based COP (BpZn-COP) upon integration with TiO_2 (TiO_2@BpZn-COP). This composite achieved a remarkable HER of 1333 μmol $g^{-1}h^{-1}$ (over eight times higher than pristine BpZn-COP) while maintaining a low AQY of 2.5 at 420 nm [40]. Reported AQYs of COPs are typically low, highlighting the need for improvement. To overcome these limitations and achieve excellent HER with high AQY at longer wavelengths (up to 500 nm), researchers focus on engineering COPs with broad light absorption, outstanding photochemical stability, high hydrophilicity, abundant active sites, and efficient charge separation [2,26,41–43].

Hydrophilicity is widely recognized as a critical factor for effective photocatalytic hydrogen production. However, a major limitation of many reported photocatalysts, including COPs, covalent organic framework (COFs), Conjugated microporous polymers (CMPs), and Conjugated polymers (CPs), is their inherent hydrophobicity, impeding efficient interaction with water during the photocatalytic reaction. Consequently, incorporating hydrophilic functional groups like hydroxyls, ethylene glycols, bipyridyl, carboxylic acids, amino acids, sulfones, or ionic electrolytes into the polymer network has become a crucial strategy to enhance both hydrophilicity and photocatalytic activity, as demonstrated in various studies [3,44–50]. While various approaches exist, Xiang et al. explored post-modification methods to integrate edge-functionalized graphene materials (EFGs) with COPs for enhanced energy storage and conversion [45].

Moreover, D-π-A systems have demonstrated strong HERs under photocatalytic activity due to the push–pull effect that enhances charge carrier separation [51–56] However, most reported polymer photocatalysts using these systems rely on expensive catalysts, unfriendly environmental conditions, and multicomponent starting material for polycondensation reactions [57–59]. A green synthetic approach based on self-condensation is needed to construct polymers with new D-π-A systems. Non-conjugated systems offer potential for photocatalytic hydrogen production, but further advancements are needed to create hydrophilic materials with rapid water reactivity and efficient light response [26,50]. Benzoin condensation could be more desirable since it satisfies atom economics and does not produce any byproducts. However, the production of benzoin-containing polymers requires toxic reagents such as potassium cyanide [60–62] and *p*-toluenesulfonic acid [63].

Herein, a green strategy is described for obtaining hydrophilic, non-conjugated, semicrystalline network benzoin-based COPs (D-π-A) with quantitative yield using multi-formyl linkers and Vitamin B1 (Thiamine. HCl) as a catalyst. To elucidate the impact of benzoin linkages and identify the optimal structure for photocatalytic performance, we directly compared the photoelectronic properties and photocatalytic activity of COPs containing benzoin linkages using different π-spacers (B-PyTT-COP and B-PyTP-COP) with a benzoin-free analog (Su-PyTT-COP). This comparison reveals the influence of the benzoin unit and π-spacers on light harvesting, charge separation, and ultimately, photocatalytic activity. The B-PyTT-COP photocatalyst exhibited high performance, with a HER of 233.81 μmol h^{-1} (77935.10 μmol $g^{-1}h^{-1}$) in the presence of ascorbic acid (AA) as sacrificial electron donor (SED) reagent and 4 wt% of H_2PtCl_6 as co-catalyst. Under this condition, this COP produces an unprecedented AQY of 60.03 %, 61.10 %, and 65.35 % at 420, 460, and 500 nm, respectively, compared to other members of the COP family. Unprecedently, among all materials evaluated, B-PyTT-COP has demonstrated an exceptional ability to generate a high AQY value at 500 nm (65.35 %). The outstanding hydrogen production efficiency and unprecedented AQY of B-PyTT-COP are attributed to its unique molecular architecture. The seamless integration of pyrene, thiophene, and benzoin components within its heterojunction structure not only fosters exceptionally efficient charge transfer but also significantly enhances proton affinity. These synergistic effects expedite intramolecular charge transfer (ICT) processes, establishing B-PyTT-COP as a promising candidate among the studied photocatalysts for driving an excellent hydrogen generation and a high apparent quantum yield. A notable feature of all benzoin-based COPs is that they can produce O_2 by using silver nitrate as a sacrificial electron acceptor (SEA).

2. Experimental procedure

2.1. Synthesis of benzoin-based COP

0.50 mL of DI water and 2 mL of EtOH 95 % were added to a test tube containing 2.7 mg (10 mmol%) of thiamine hydrochloride (Vitamin B1). The mixture was cooled in an ice bath. 0.3 mL of a cold NaOH 6 M solution was added dropwise within 7–10 mins. to this solution. The pH was adjusted to 8.0. Then 0.080 mmol of multiformyl derivatives (TriFPB-3CHO, TPA-3CHO, TFPB-4CHO, PyTP-4CHO, and PyTT-4CHO) were added to the reaction mixture. It was sonicated for 15 mins. and then heated in an oil bath at 60 °C for either 24 h or 72 h. The reaction mixture was cooled to room temperature and left standing for 12 h. The solid was obtained after filtration and washing with 20 mL of ice-cold water/ethanol (1:1 v/v), and THF, respectively. Finally, the solid was extracted using Soxhlet with methanol (MeOH) for 24 h. The resulting benzoin-based COP (B-PyTT-COP, B-PyTP-COP, B-TFPB-COP, B-TPA-COP, or B-TriFPB-COP) was dried in an oven at 120 °C for 12 h and obtained with a quantitative yield (100 %) (Scheme 1). For more details about each COP, refer to the section titled “Synthetic procedure of COPs with benzoin linkage” in Supplementary Information.

2.2. Photocatalytic hydrogen generation

The experiment was carried out on a photocatalytic reaction cell (245 mL). 3 mg of benzoin-based COP powder was dispersed in 10 mL of a mixed solution of 80 vol% H_2O, 20 vol% MeOH, 0.1 M of AA as SED, and 4 wt% H_2PtCl_6 (1.9 wt% Pt) as co-catalyst. Also, the photocatalytic reaction works without co-solvent (MeOH) as follows: 3 mg of benzoin-based COP powder was dispersed in 10 mL of a mixed solution of 100 vol % H_2O in the presence of 0.1 M of AA as SED, and 4 wt% H_2PtCl_6 (1.9 wt % Pt) as co-catalyst. It was further ultrasonicated for 5 min to obtain a well-dispersed suspension. The resulting suspension was degassed using Argon gas for 10 min to ensure complete air removal before irradiation with a 350 W Xe light source (1000 Wm^{-2}; λ = 380–780 nm) under stirring. The reaction time was 4 h at ambient temperature by a stream of cold water. Ensuring of H_2 production was thermally detected via bit injection by a semi-capillary column (molecular sieve; diameter: 8 mm; length: 3 m) into the reactor headspace gas (0.5 μL) into a gas chromatograph (GC7920) under isothermal parameters. Furthermore, a 350 W Xe lamp with different band-pass filters of 420, 460, 500, 550, 600, and 650 nm with light intensity ranging from 60 to 100W cm^{-2} was used to measure the AQY (Fig. S53). The apparent quantum yield (AQY) was calculated using the following equations:

$$AQY = \frac{number\,of\,evolved\,H_2\,molecules \times 2}{number\,of\,incident\,photons} = \frac{N_e}{N_P} = \frac{2M \times N_A}{\frac{E_{total}}{E_{photon}}}$$

$$= \frac{2M \times N_A}{\frac{S \times P \times t}{h \times \frac{c}{\lambda}}} = \frac{2M \times N_A \times h \times c}{S \times P \times t \times \lambda} \times 100\%$$

where N_A is the Avogadro constant, M is the amount of H_2 produced (mol), c is the speed of light h is the Planck constant, S is the irradiation area (cm^2), t is the photoreaction time (s), P is the intensity of the irradiating light (60-100W cm^{-2}), and λ is the wavelength of the monochromatic light (m).

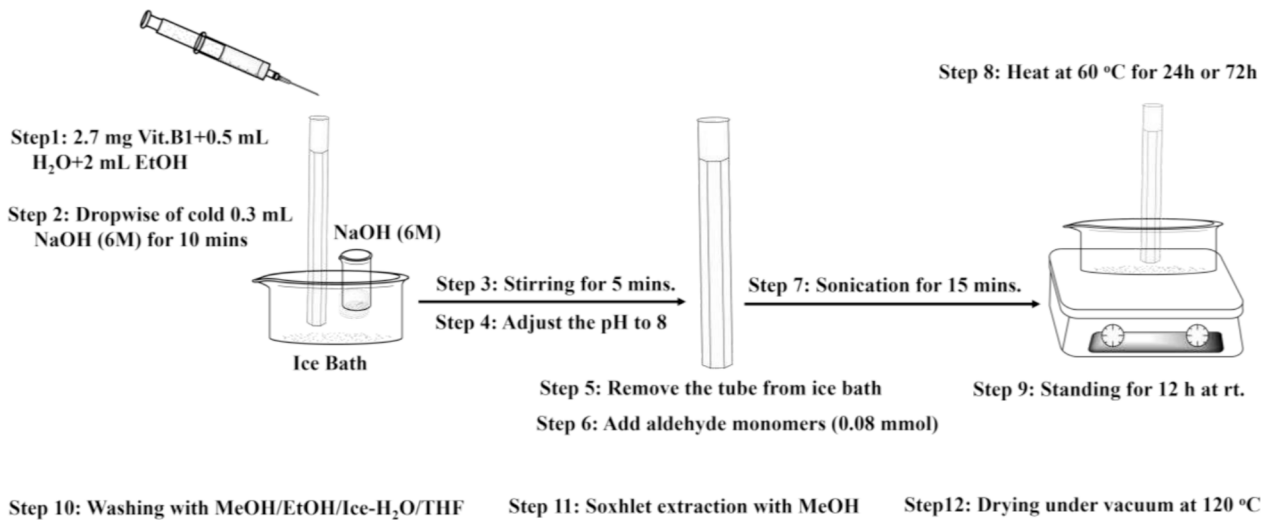

Scheme 1. Schematic representation of preparation steps for benzoin-based COP.

3. Results

3.1. COP synthesis and characterization

For the first time, this work demonstrates the feasibility of preparing hydrophilic, non-conjugated linkage, and D-π-A structured COPs using a green benzoin condensation approach to enhance photocatalytic hydrogen production and AQY. We synthesized a series of three-coordinates triformyl compounds, including 4,4′,4″-Triformyltriphenylamine (triphenylamine, TPA-3CHO) and 4,4′,4′′-(benzene-1,3,5-triyl)-trisbenzaldehyde(triphenyl-benzene, TriFPB-3CHO), as well as four-coordinates tetraformyl moieties such as 4,4′,4′′,4′′′-(pyrene-1,3,6,8-tetrayl)tetrabenzaldehyde (tetraphenylpyrene, PyTP-4CHO), 5,5′,5′′,5′′′-(pyrene-1,3,6,8-tetrayl)tetrakis(thiophene-2-carbaldehyde) (tetrathienylpyrene, PyTT-4CHO), and 4,4′,4′′,4′′′-(benzene-1,2,4,5-tetrayl)-trisbenzaldyde (tetraphenyl benzene, TFPB-4CHO), through formylation reactions and Suzuki coupling reactions with suitable precursors (**Synthetic procedure** and Figs. S1-

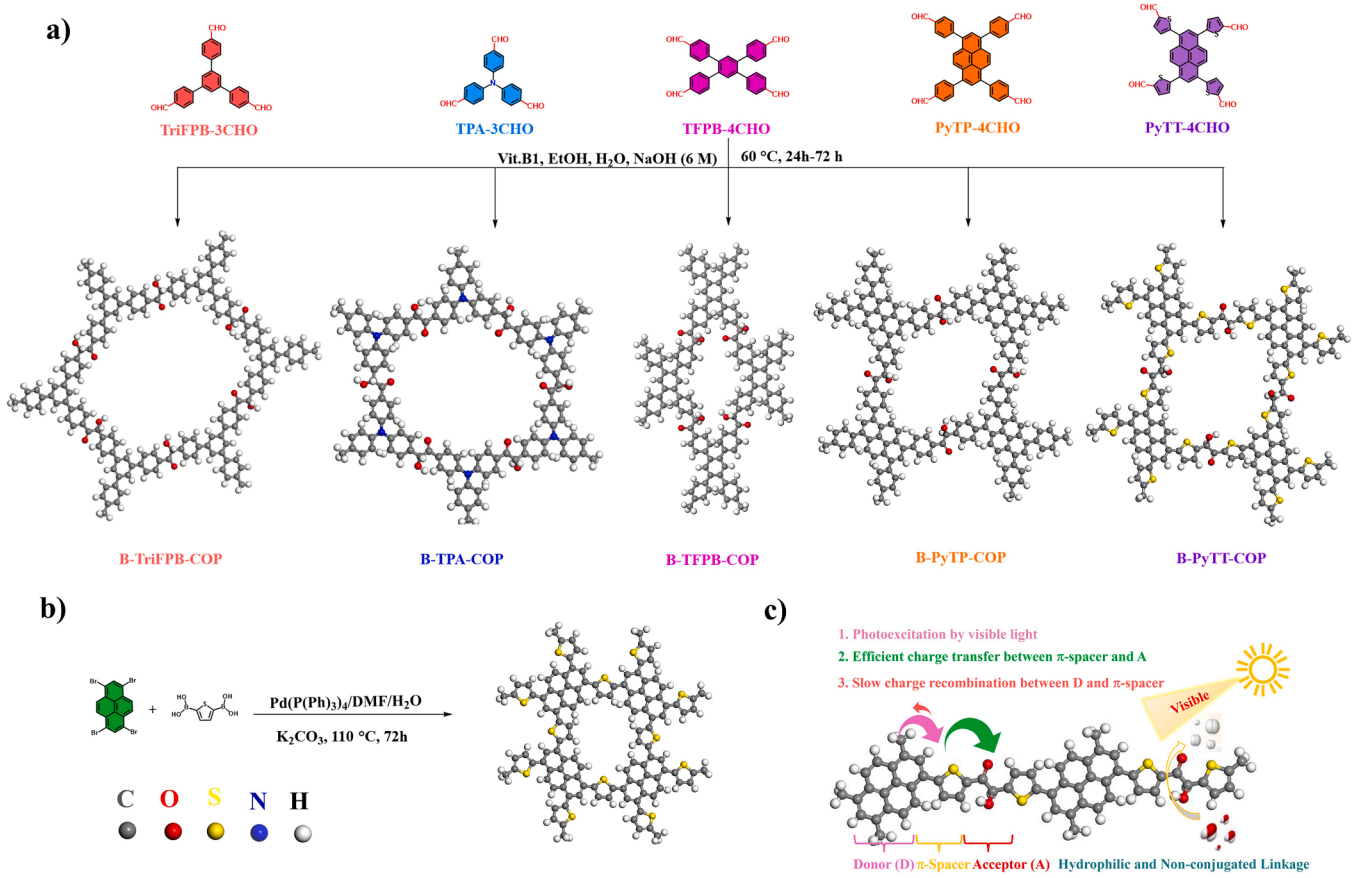

Fig. 1. Schematic representation of the possible Structures of COPs through benzoin condensation in the presence of Vit.B1 as a catalyst (a). Synthesis of COP based on Suzuki coupling (b). Schematic diagram illustrates the charge transfer through the B-PyTT-COP chain during the photocatalytic reaction under visible light (c).

S8, and S12-S16). Moreover, a one-pot green benzoin condensation strategy was developed to produce a series of five novel hydrophilic COPs with non-conjugated α-hydroxyl ketone linkage (i.e., benzoin-based COPs). Multiformyl monomers were dissolved in an ethanol–water solvent system with an alkaline medium, using thiamine HCl (vitamin B1) as a green catalyst (Fig. 1a). Reaction conditions were optimized across various solvents (EtOH, MeOH, THF, DMF, toluene, and acetonitrile). EtOH provided the highest yield and quality for B-TFPB-COP synthesis (Fig. S17). B-TFPB-COP, B-TPA-COP, and B-TriFPB-COP achieved quantitative yields within 24 h at 60 °C. However, B-PyTT-COP and B-PyTP-COP required 72 h at the same temperature, due to the increased complexity of the pyrene moiety. This green strategy utilizes vitamin B1 as a mild, efficient, and selective catalyst for the benzoin condensation reaction, a key method in small molecule synthesis [64,65]. The thiazolium ring in vitamin B1 serves as the active site, enhancing the acidity of an adjacent hydrogen atom. A base can then easily remove this hydrogen, forming a carbanion. This carbanion subsequently attacks another an aldehyde molecule, creating a new C—C bond. The simplicity of this benzoin-based COP synthesis is remarkable, relying on self-condensation, a green catalyst, a single monomer, mild conditions, and short reaction times [66]. Moreover, after polymerization, the catalyst was efficiently removed by continuous washing with ice water/ethanol and THF. To validate our concept, one COP free benzoin linkage was prepared using a conventional method such as Suzuki coupling (Su-PyTT-COP) (Fig. 1b). To investigate the effects of benzoin linkage insertion on the resultant COPs properties, we focused on preparation techniques, photoelectric characteristics, and photocatalytic activity. Furthermore, all as-prepared benzoin-based COP incorporate hydrophilic, non-conjugated linkage with D-π-A system. As shown in Fig. 1c, B-PyTT-COP demonstrates optimal structure for enhancing photocatalytic hydrogen evolution. This exceptional activity likely arises from the synergistic combination of pyrene (acting as a strong donor), thiophene (π-spacer promoting for efficient light harvesting), and the benzoin linkage (functioning as hydrophilic, non-conjugated linkage and strong acceptor that facilitates efficient charge transfer). This synergy ultimately leads to outstanding HER and unprecedented AQY.

FTIR analysis confirmed the successful incorporation of α-hydroxyl ketone linkages (benzoin linkages) in all synthesized benzoin-based COPs by comparison with their monomers (Fig. 2a–c and Figs. S18 and S19). Notably, the characteristic carbonyl peak intensity (1663–1700 cm^{-1}) significantly decreased due to benzoin condensation in the COPs network, while new bands emerged at 3373–3455 cm^{-1} (OH-stretching), 2922–2969 cm^{-1} (CH-aliphatic), and 1052–1101 cm^{-1} (C—O), confirming the presence of the benzoin linkage. Additionally, peaks at 1052 cm^{-1} (C—S) and 1324–1242 cm^{-1} (C—N) in B-PyTT-COP and B-TPA-COP, respectively, indicated the successful incorporation of thiophene and triphenylamine units (Fig. 2a and Fig. S19). Solid-state ^{13}C CP/MAS NMR spectroscopy provided further structural confirmation. Peaks within 140.70–130.80 ppm were attributed to aromatic carbons, while those within 191.2–193.16 ppm confirmed the presence of α-hydroxyl ketone carbonyl groups (Fig. 2d–f and Figs. S9 and S10).

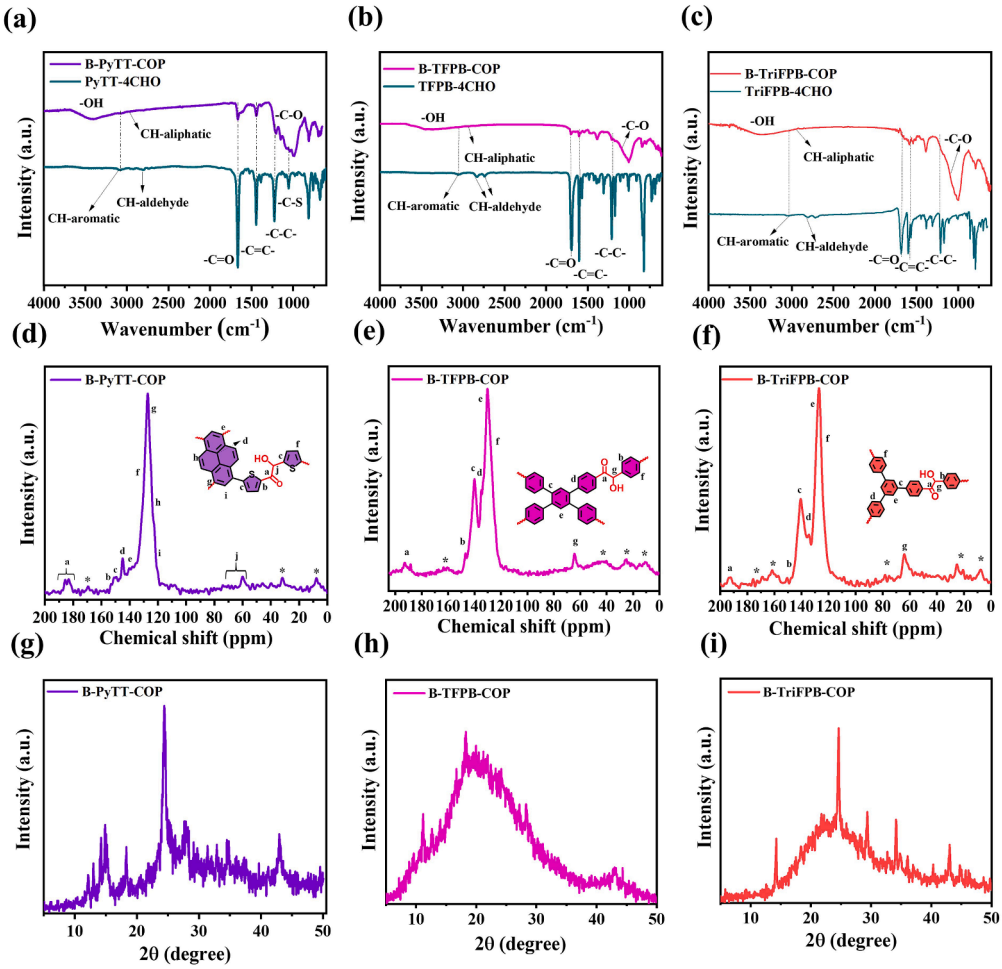

Fig. 2. FTIR spectra of B-PyTT-COP and PyTT-4CHO (a), B-TFPB-COP and TFPB-4CHO (b), and B-TriFPB-COP and TriFPB-4CHO (c). Solid-state CP-MAS ^{13}C NMR spectra of B-PyTT-COP (d), B-TFPB-COP (e), and B-TriFPB-COP (f), spinning sidebands are denoted with asterisks. XRD profiles of B-PyTT-COP (g), B-TFPB-COP (h), and B-TriFPB-COP (i).

Additionally, peaks between 60.59–68.85 ppm indicated α-hydroxyl carbon atoms. Notably, B-PyTT-COP and B-PyTP-COP displayed distinct peaks associated with the benzoin carbonyl (183.44–192 ppm) and thiophene carbon (144 ppm) [57,67] (Fig. 2d and Fig. S9). Conversely, Su-PyTT-COP, lacking the benzoin linkage, exhibited a peak at 142.80 ppm assigned to carbon atoms attached to sulfur within thiophene rings, along with overlapping pyrene and thiophene carbon peaks at 126.76 ppm (Fig. S11).

Powder X-ray diffraction (PXRD) revealed that all benzoin-based COPs had a semicrystalline nature with semi-ordered layer arrangements in their networks (Fig. 2g–i, Figs. S21 and S22). Notably, B-PyTT-COP exhibited sharp diffraction peaks at 25° (2θ), suggesting ordered stacking of pyrene moieties and potentially enhanced charge transport. In contrast, the amorphous structure was observed for free benzoin analog (Su-PyTT-COP) (Fig. S23). The thermogravimetric analysis (TGA) demonstrated the high thermal stability of benzoin-based COPs (Fig. S24). The N_2 sorption measurements confirmed type II isotherm with Brunauer–Emmett–Teller (BET) surface areas ranging from 19.04 to 85.00 m^2/g and permanent pore size from 2 to 10 nm (Figs. S25 and S26). Scanning electron microscopy (SEM) and transmission electron microscopy (TEM) images showcased diverse morphologies, including rod-like structures (B-PyTT-COP and B-TriFPB-COP), flake-like structures (B-TPA-COP and B-TFPB-COP), and layered structures (B-PyTP-COP) (Figs. S27 and S28). Energy-dispersive spectroscopy (EDX) analysis confirmed the presence of expected elements (C, N, S, O, Pd) and the purity in all benzoin-based COPs (Fig. S29).

X-ray photoelectron spectroscopy (XPS) measurements for COPs with and without benzoin linkage confirmed the different chemical environments for C, N, O, and S atoms (Fig. 3a). Analysis of high-resolution XPS spectra for C 1s, N 1s, O 1s, and S 2p core levels provided further insights. The core level C 1s of B-PyTT-COP deconvoluted at 2.83.34, 287.70, and 291.19 eV, attributable to C═C (sp^2 hybridized carbon)/C—C (sp^3 hybridized carbon), C═O, and C—O/C—S, respectively (Fig. 3b). The core level O 1s of B-PyTT-COP display peaks at 530.48 and 531.60 eV assignable to C═O and C—O(OH), confirming the formation of benzoin linkages (Fig. 3c). Fig. 3d depicted the deconvolution S 2p core-level peaks of B-PyTT-COP at 162.82 eV and 163.75 eV, corresponding to S $2p_{1/2}$ and S $2p_{3/2}$. Furthermore, Fig. 3e and f examined the C 1s and S 2p core levels for Su-PyTT-COP. A list of high-resolution XPS spectrums for the other benzoin-based COPs is provided in Fig. S30. To assess the impact of benzoin linkage on hydrophilicity, we measured water contact angles of benzoin-containing B-PyTT-COP and its benzoin-free counterpart Su-PyTT-COP (Fig. 3d). Thin films were prepared on glass substrates via drop-casting. B-PyTT-COP exhibited a significantly lower initial contact angle (55°) than Su-PyTT-COP (124.1°). Furthermore, B-PyTT-COP demonstrated rapid wetting, with the angle decreasing to 7° after 0.5 min and 2° after 10 min. In contrast, Su-PyTT-COP maintained a much higher contact angle (114.3°) even after 10 min. These results clearly demonstrate the enhanced hydrophilicity of benzoin-based COPs (Fig. S31). Enhanced hydrophilicity promotes water interaction during photocatalysis, as evidenced by the Tyndall effect and DLS analysis confirming the colloidal structure of solutions (Fig. S32). Furthermore, atomic force microscopy (AFM) revealed B-PyTT-COP's surface roughness (Rq = 26 nm, Ra = 19 nm), suggesting potential proton reaction sites during photolytic reaction (Fig. S33).

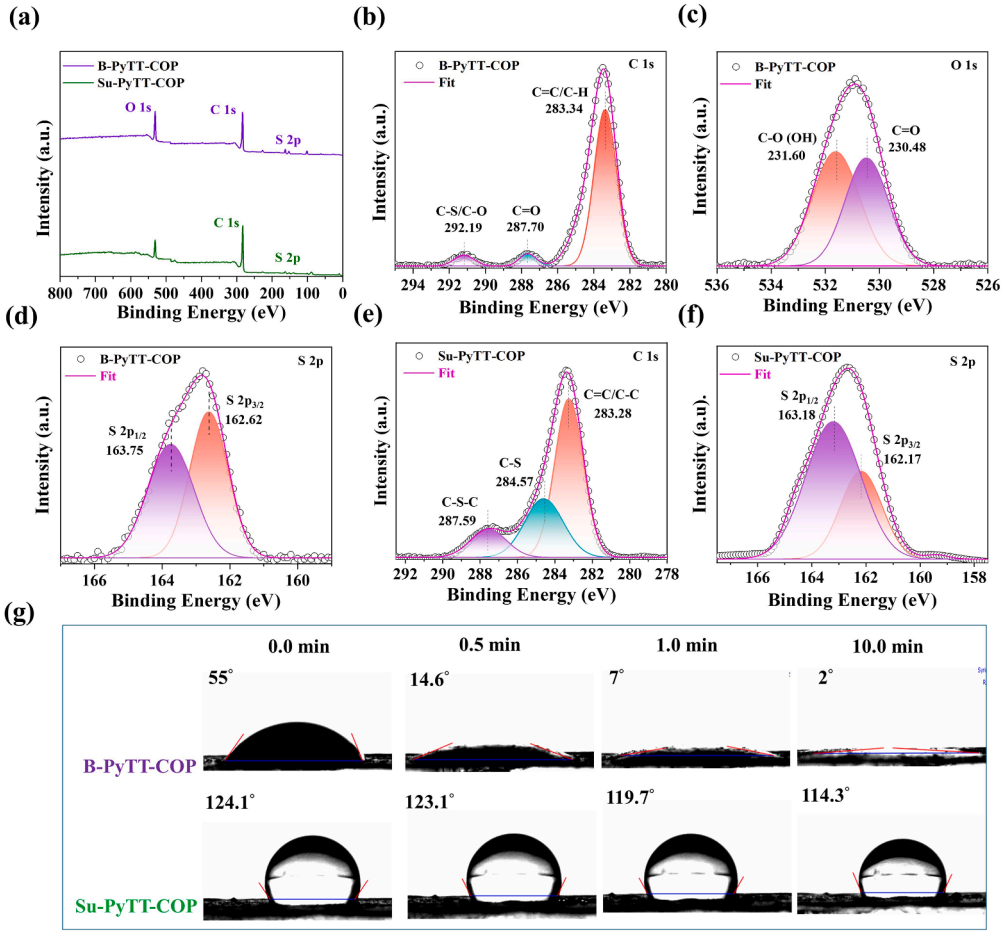

Fig. 3. The survey XPS of B-PyTT-COP, and Su-PyTT-COP (a). High-resolution spectra for C 1s (b), O 1s (c), and S 2p (d) of B-PyTT-COP, respectively. High-resolution spectra for C 1s (e), and S 2p (f) of Su-PyTT-COP, respectively. Time-dependent water contact angles without light illumination of B-PyTT-COP, and Su-PyTT-COP (g).

3.2. Photoelectronic properties of COPs with and without benzoin linkage

Ultraviolet/visible diffuse reflectance spectroscopy (UV–Vis DRS), ultraviolet photoelectron spectroscopy (UPS), steady-state photoluminescence spectroscopy (PL), time-correlated single photon counting (TCSPC), electron paramagnetic resonance (EPR), and electrochemical impedance spectroscopy (EIS) were used to investigate the critical role of benzoin linkage and π-spacer integration in photoelectronic properties of B-PyTT-COP, B-PyTP-COP, and Su-PyTT-COP. The UV–Vis DRS spectra of the three COPs with and without benzoin linkage are shown in Fig. 4a. The absorption curves of the COP with benzoin linkage exhibit a redshift initially when incorporating thiophene with benzoin linkage (B-PyTT-COP), followed by a blueshift upon integrating benzene with benzoin linkage (B-PyTP-COP), in comparison to Su-PyTT-COP. This behavior can be attributed to the ability of thiophene to enhance conjugation. Thiophene's extended π-electron system facilitates efficient electron delocalization within the molecule. As a result, incorporating thiophene between the pyrene units extends the overall conjugation length, leading to a redshift in the absorption spectrum [68,69]. In contrast, B-PyTP-COP, which integrates benzene rings instead of thiophene, displays a blueshift compared to B-PyTT-COP. While benzene possesses some degree of conjugation, its electron delocalization efficiency is lower compared to thiophene. This difference translates to a shorter conjugation length in B-PyTP-COP, resulting in a blueshift of the absorption edge. B-PyTT-COP demonstrates the broadest light absorption range, resulting in the smallest bandgap of 1.98 eV, which can be beneficial for enhancing photocatalytic reactions under visible light. Based on the Tauc plots, it has been calculated that the optical band gaps of B-PyTT-COP, B-PyTP-COP, and Su-PyTT-COP are 1.98, 2.18, and 2.05 eV, respectively (Fig. S35). The band gap of B-PyTT-COP might catalyze the reduction of H_2O to H_2 effectively compared to other two COPs (B-PyTP-COP and Su-PyTT-COP) (Table 1). Moreover, UPS was utilized to study the energy levels of these COPs (Fig. 4b, Fig. S37). The valence band maximum (VBM) and conduction band minimum (CBM) of B-PyTT-COP, B-PyTP-COP, and Su-PyTT-COP were −5.72/−3.74, −6.31/−4.13, and −5.01/−2.96, respectively (Fig. 4b, Table 1). The CBM of all the COPs was higher than the reduction potential of H_2, which means that these catalysts could potentially split water to produce hydrogen. Interestingly, the VBM of B-PyTT-COP and B-PyTP-COP are 5.72 and 6.31, As a result, these photocatalysts might also be used to produce O_2 respect with the Su-PyTT-COP (Fig. 4b, Figs. S37 and S38, and Table 1) [70]. Moreover, the PL-spectra of the three COPs excited at 400 nm showed different emission bands and intensities. The emission intensity of B-PyTT-COP was lower than the other two COPs (B-PyTP-COP and Su-PyTT-COP) (Fig. 4c). This suggests that B-PyTT-COP is more efficient at generating charge carriers and suppressing exciton recombination, both critical factors for photocatalytic activity. Furthermore, we utilized TCSPC to estimate the excited-state lifetimes for these COPs (Fig. 4d and Table S2). The average fluorescence lifetimes of the B-PyTT-COP, B-PyTP-COP, and Su-PyTT-COP were calculated to be 0.702, 0.498, and 0.436 ns, respectively, which correlates with the higher photocatalytic performance observed for B-PyTT-COP. Electrochemical impedance spectroscopy (EIS) and electron paramagnetic resonance (EPR) were used to investigate free electron radical generation in COPs. A strong signal was observed at 3489–3528 gauss, due to the presence of radicals. As light irradiation increased, the intensity of the EPR signal increased, indicating more radicals were generated. The B-PyTT-COP showed a more excellent irradiation-induced signal enhancement than the other COPs (Fig. 4e). This suggests that the engineered structure of B-PyTT-COP, incorporating pyrene, thiophene, and benzoin linkages, promotes both light harvesting and radical generation. The EIS data also showed that the charge transfer resistance value of B-PyTT-COP was lower than those of B-PyTP-COP and Su-PyTT-COP (Fig. 4f). The findings imply that B-PyTT-COP possesses a more favorable interface for charge transfer, a critical factor for photocatalytic hydrogen production [71]. As a result, the continuous heterojunction structure of pyrene moieties, thiophene,

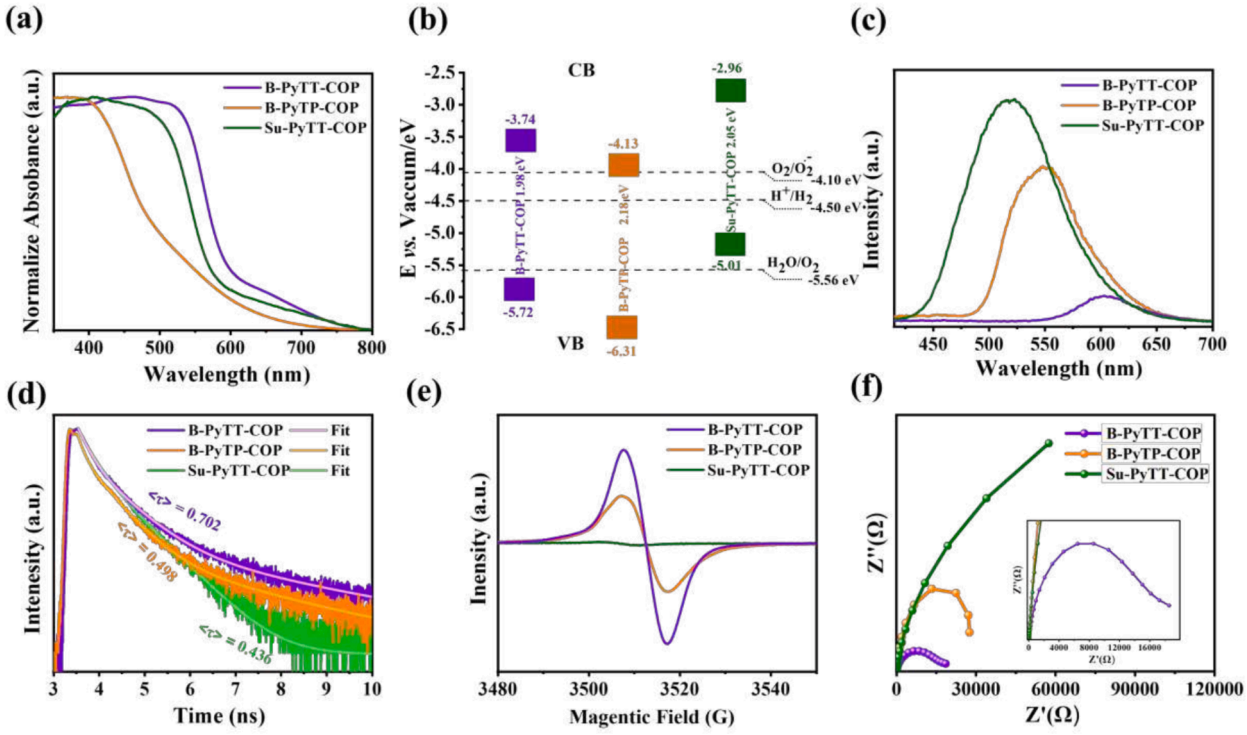

Fig. 4. Diffuse reflectance UV–Vis spectra (a), Band diagram and their thermodynamic equilibrium redox potentials for O_2 and proton reduction and H_2O oxidation in vacuum scale (b), PL emission spectra in *N*-methylpyrrolidine; excitation wavelength (400 nm) (c), TCSPC spectra (d), EPR spectra were collected in the solid state under additional light illumination (e), Electrochemical impedance spectra (EIS) were measured at 1.5 V vs. Ag/AgCl electrode under light irradiation (LED lamp; λ > 420 nm) in 0.5 M Na_2SO_4 as the electrolyte (f) of B-PyTT-COP, B-PyTP-COP, and Su-PyTT-COP.

Table 1
Photophysical Properties and HERs of the COPs with and without benzoin linkage.

COPs	HOMO/ LUMO (eV) [a]	Absorption onset (nm)[b]	Optical gap (eV)[c]	HER (μmol h^{-1})[d]	HER (μmol h^{-1})[e]	AQY%[f] 420	460	500
B-PyTT-COP	−5.72/-3.74	626.00	1.98	233.81	164.10	60.03	61.10	65.35
B-PyTP-COP	−6.31/-4.13	516.00	2.18	6.24	3.10	2.00	1.50	1.00
Su-PyTT-COP	−5.10/-2.96	710.00	2.05	0.55	0.022	0.32	0.10	0.003

[a] HOMOs determined using UPS; LUMOs derived from the expression $E_{HOMO} - E_g$.
[b] Absorption onsets from UV–Vis DRS spectra.
[c] Band gaps calculated from Tauc plots.
[d] Conditions: 3 mg of COP powder and 10 mL of a mixed solution consisting of 80 vol% H_2O, 20 vol% MeOH, 0.1 M of AA as SED, and 4 wt% H_2PtCl_6 (1.9 wt% Pt) as co-catalyst, measured under 350-W Xe light (λ = 380–780 nm; 1000 W m^{-2}).
[e] Conditions: 3 mg of COP powder and 10 mL of a mixed solution consisting of 100 vol% H_2O, 0.1 M of AA as SED, and 4 wt% H_2PtCl_6 (1.9 wt% Pt) as co-catalyst, measured under 350-W Xe light (λ = 380–780 nm; 1000 W m^{-2}).
[f] AQYs measured at 420, 460, and 500 nm.

and benzoin linkage accelerated the rate of intramolecular charge transfer (ICT) and increased the affinity of the COP for protons [72–74]. This indicates that B-PyTT-COP is the most efficient photocatalyst for hydrogen production (Table 1). Besides, the UV-DRS, Tauc plot, UPS, and band structure for B-TFPB-COP, B-TriFPB-COP, and B-TPA-COP were mentioned in Supporting Information (Figs. S34, S36, S37 and

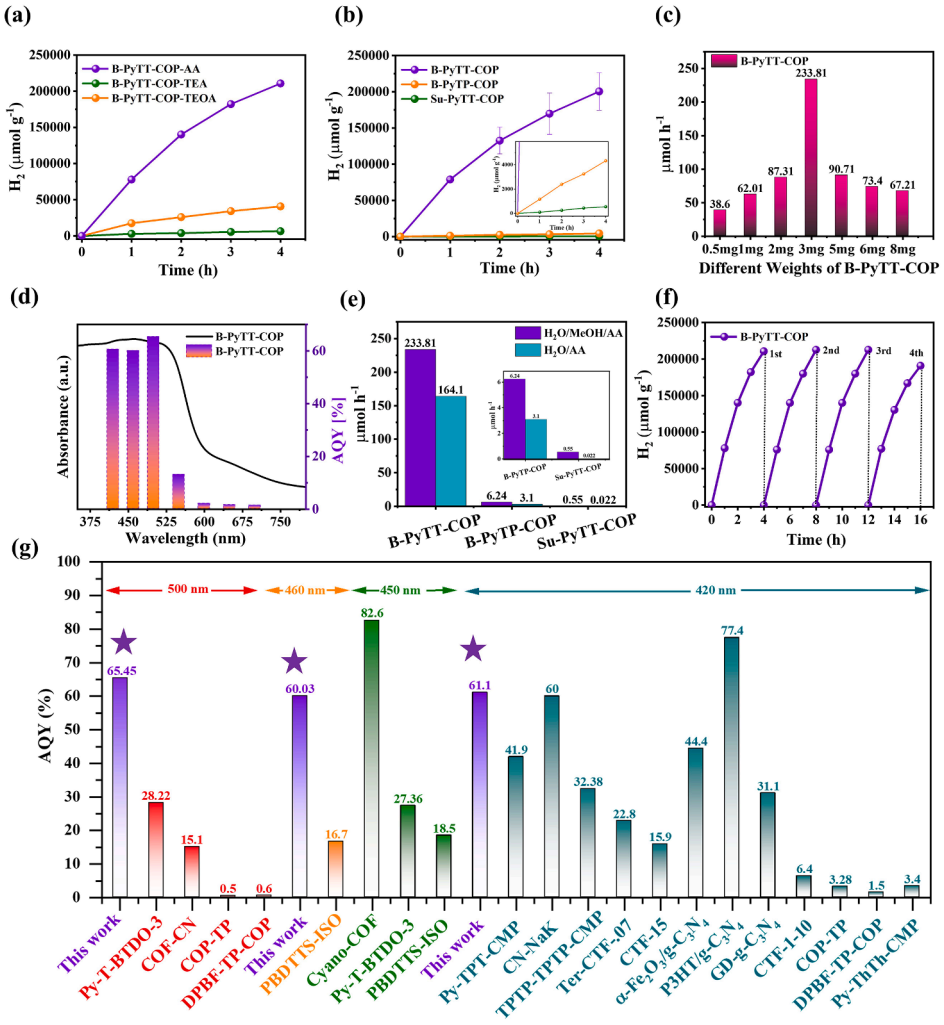

Fig. 5. The HER of B-PyTT-COP using different SEDs (a). Time-dependent HER (b) of B-PyTT-COP, B-PyTP-COP, and Su-PyTT-COP photocatalysts under 380–780 nm irradiation (3 mg of COP powder and 10 mL of a mixed solution consisting of 80 vol% H_2O, 20 vol% MeOH, 0.1 M of AA as SED, and 4 wt% H_2PtCl_6 (1.9 wt% Pt) as co-catalyst). HERs (c) of the B-PyTT-COP were measured at different weights. Correlation between the apparent quantum yield (AQY) and the UV–vis absorption spectra (d) of B-PyTT-COP. HER values in the absence of MeOH (i.e., in a 100 vol% H_2O in the presence of 0.1 M of AA as SED) (e) of B-PyTT-COP, B-PyTP-COP, and Su-PyTT-COP compared to the HER values in the presence of MeOH (i.e., 80 vol% H_2O, 20 vol% MeOH, and 0.1 M of AA as SED). The HER stability (f) of B-PyTT-COP for 20 h (3 mg of COP powder and 10 mL of a mixed solution consisting of 80 vol% H_2O, 20 vol% MeOH, 0.1 M of AA as SED, and 4 wt% H_2PtCl_6 (1.9 wt% Pt)), λ = 380–780 nm). The sample was degassed after each 4 h to prevent detector saturation. AQY% comparison between this work at 420, 460, and 500 nm and reported works (g).

S38).

3.3. Photocatalytic H_2 evolution of COPs with and without benzoin moieties

To evaluate the hydrogen evolution reaction (HER) of the synthesized COPs, we utilized a Xenon lamp emitting light across a broad spectrum ranging from 380 to 780 nm. In our experimental procedure, we dispersed 3.0 mg of each COP powder into a 10 mL solution of H_2O/MeOH in a (4:1; v/v). Ascorbic acid (AA) was selected as the best sacrificial electron donor (SED) after a thorough evaluation of various other potential reagents [75], including triethanolamine (TEOA) and triethylamine (TEA), as illustrated in Fig. 5a. Also, the highest HER was observed when AA was employed in the presence of 4 wt% H_2PtCl_6 as the co-catalyst. B-PyTT-COP produced a high hydrogen evolution rate (HER) in the first hour up to 233.81 μmol h^{-1} (77,935.1 μmol $g^{-1}h^{-1}$) during the photocatalytic reaction. Interestingly, the HER of B-PyTT-COP has also been compared to the results reported in the literature for other polymeric materials, including CPs, CMPs, COPs, COFs, MOFs, and g-C_3N_4 (Table S5). It was found that B-PyTT-COP had a 37 and 232-fold higher H_2 evolution rate than B-PyTP-COP (6.24 μmol h^{-1}) and Su-PyTT-COP (0.55 μmol h^{-1}), respectively (Fig. 5b). The presence of benzoin linkage in B-PyTT-COP promotes photocatalytic hydrogen evolution reaction (HER). This is attributed to the B-PyTT-COP has excellent separation of photogenerated holes and electrons, more hydrophilic character, strong absorption in the visible region, and strong interactions between the π orbitals of the pyrene-thiophene moieties as donor-π-spacer and benzoin bridge as acceptor [57]. Therefore, the integration of thiophene as a π-spacer is essential for obtaining excellent HER. Furthermore, we precisely adjusted the quantity of H_2PtCl_6 utilized as a co-catalyst (2,4, and 7 wt%) and examined its impact on the photocatalyst to enhance hydrogen production in the AA solution (Figs. S39–S43).

Additionally, seven different weights of the B-PyTT-COP were tested (0.5, 1.0, 2.0, 3.0, 5.0, 6.0, and 8.0 mg) and 3.0 mg was the best HER (Fig. 5c). When the dosage of the B-PyTT-COP was elevated from 0.5 to 3.0 mg, the HER increased markedly to reach 233.81 μmol h^{-1} (Fig. 5c and Figs. S39–S43). However, when the dosage was increased from 3 to 8 mg, the HER rapidly dropped to reach 67.21 μmol h^{-1}. The higher HER observed with 3 mg of B-PyTT-COP catalyst in Fig. 5c compared to other weights can be attributed to a balance between light absorption and active site utilization. While a low catalyst amount limits light capture, exceeding the optimal loading such as 5, 6, and 8 mg, leads to overcrowding and light scattering. This reduces the light reaching active sites on the catalyst particles, hindering their ability to participate in the hydrogen evolution reaction. Therefore, 3 mg provides the optimal balance, allowing for efficient light absorption and utilization of a significant number of active sites for hydrogen production. Elevated quantities of COPs within a reaction solution lead to accelerated particle aggregation, causing diminished light absorption and transmission [76–78]. Therefore, as the mass of COPs photocatalyst increases, the HER decreases.

It is worth mentioning that the apparent quantum yields (AQYs) of the B-PyTT-COP were explored using band-pass filters that isolated single wavelengths including, 420, 460, 500, 550, 600, and 650 nm. Remarkably, B-PyTT-COP demonstrated unprecedentedly high AQY values, recording 60.03 %, 61.10 %, and 65.35 % at 420, 460, and 500 nm, respectively. Until now, these performances surpassed all tested materials related to the COPs family. To our knowledge, B-PyTT-COP exhibits an exceptional ability to achieve a high AQY value of 65.35 % at 500 nm, surpassing all previously examined materials (Fig. 5g, Table S5). After 500 nm, the AQY decreased as the wavelength of the irradiation light increased, which agrees well with the light absorption properties of B-PyTT-COP (Fig. 5d). Moreover, to ensure the accuracy of AQY measurements, we optimized the AQY at 500 nm using a wide range of photocatalyst concentrations (1–8 mg) and found that the stationary point of B-PyTT-COP is at 3 mg, with an AQY of 65.35 % (Fig. S45). In addition, benzoin-based COP showed a good AQY of 2.2 % even when irradiated with a red light at 600 and 650 nm, demonstrating its high efficiency in photocatalytic HER. Moreover, B-PyTT-COP had better AQY values at different wavelengths (λ = 420,460, and 500 nm) (Table 1).

In terms of hydrophilicity of benzoin-based COPs, the HER performance of B-PyTT-COP, B-PyTP-COP, and Su-PyTT-COP without methanol as a co-solvent (i.e., with 100 vol% H_2O/0.1 M AA as SED and 4 wt % H_2PtCl_6 as co-catalyst; Fig. 5e) was investigated. Su-PyTT-COP demonstrated very low HERs (0.022μmol h^{-1}), while B-PyTT-COP and B-PyTP-COP achieved high values of 164.10 and 3.10μmol h^{-1}, respectively. Notably, these values were consistent with those achieved in the presence of methanol as co-solvent (233.81 and 6.24μmol h^{-1} for B-PyTT-COP and B-PyTP-COP, respectively). Furthermore, water contact angle measurements consistently demonstrate that the benzoin-based COPs are super-hydrophilic compared to Su-PyTT-COP (Fig. 3g, Fig. S31). This suggests a strong correlation between the presence of the benzoin linkage and enhanced hydrophilicity, which likely plays a crucial role in the superior HER performance of the benzoin-based COPs. Fig. 5f depicts the long-term stability experiment using B-PyTT-COP, which showed no obvious decline in H_2 production for 20 h. FT-IR analysis (Fig. S49) revealed nearly identical spectra for B-PyTT-COP before and after photocatalysis, highlighting its outstanding stability during the photocatalytic reaction. Also, the photocatalytic hydrogen evolution of as-prepared COP with and without benzoin linkage was tested without additional co-catalyst (i.e. just based on the Pd-residual). B-PyTT-COP and Su-PyTT-COP have Pd contents of 0.025 and 0.103 wt %, respectively. There is no linear relationship between residual Pd content and HER value (Fig. S47). Our findings suggest that variations in photocatalytic activity of the COPs primarily stem from differences in their microstructures, rather than solely depending on their Pd content.

Systematic evaluation of each component in our photocatalytic HER system, including water, benzoin-based COP catalyst, light source (380–780 nm), Pt-cocatalyst, and SED, was achieved through comprehensive experiments and optimization steps. The absence of these components led to no H_2 observation for up to 4 h, highlighting their crucial roles (Fig. S41a). D_2O solvent and GC-Mass analysis confirmed water as the H_2 source (Fig. S41b). It is worth mentioning that research groups and catalyst systems differ significantly in reaction conditions, including light source, photocatalyst mass, and reactor characteristics [79,80]. Also, the methods reported for evaluating photocatalysts are not sufficient or uniform. To achieve more accurate HER and AQY, we followed all recent considerations [76,81].

3.4. Thin-Film H_2 evolution of COPs with and without benzoin moieties

To investigate the thin-film HER, we coated the Pt-loaded B-PyTT-COP by drop cast cycle and irradiated the substrate in the presence of 100 vol% H_2O and 80 vol% H_2O/20 vol% MeOH, respectively, (Fig. 6a and b). HER was observed for the B-PyTT-COP with the FTO-substrate in the absence and presence of MeOH, respectively (3.53 and 3.27 mmol $m^{-2}h^{-1}$) Fig. 6c and 6d. Moreover, using a silicon wafer in the absence and presence of MeOH reduced the HER to 0.89 and 0.80 mmol $m^{-2}h^{-1}$. Also, adding methanol to FTO and silicon wafer substrates can reduce HER, a finding confirmed by Bahnemann et al [82] and Cheng et al [83]. B-PyTT-COP on the FTO-substrate exhibits more than two times the HER of B-PyTT-COP on silicon wafers. Further demonstrating the photocatalytic activity and stability of the COPs with and without the benzoin bridge (B-PyTT-COP and Su-PyTT-COP) thin-films, we directly measured the Su-PyTT-COP's photocatalytic activity. No HER was detected in Su-PyTT-COP thin films in photocatalytic solution under light illumination (Fig. 6e). Overall, these results suggest that integrating the hydrophilic benzoin linkage into COP networks promotes strong binding to FTO. This strong binding can be attributed to the benzoin linkage's high electronegativity [84].

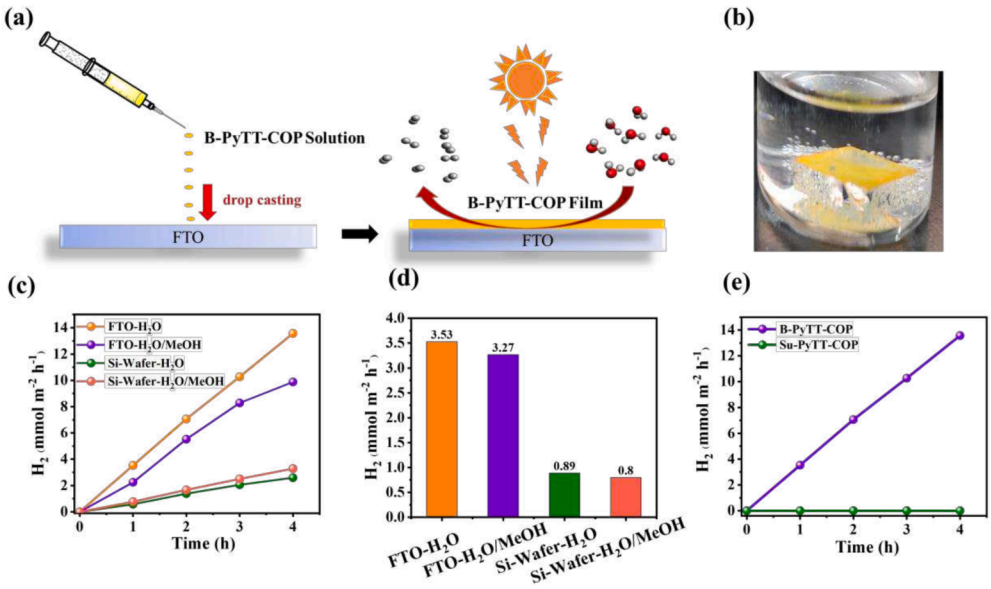

Fig. 6. Schematic illustration of the photocatalytic hydrogen evolution in film systems (a). Image of the 1 × 1.5 cm^2 film over B-PyTT-COP using FTO as substrate (b). Time-dependent HER (c) and HER of films (d) based on FTO and Si-Wafer immersed in 10 mL of a H_2O/AA and/or 10 mL H_2O/MeOH/AA solution under 380–780 nm irradiation. Thin-film HER using FTO (e) of B-PyTT-COP and Su-PyTT-COP.

3.5. Efficient charge separation and transfer driven by Benzoin-based COPs

Femtosecond transient absorption (fs-TA) spectroscopy was used to investigate the photocatalytic reaction mechanisms of COPs with and without benzoin linkages. The excitation wavelength used for these photocatalysts was 460 nm, corresponding to their specific band structures. Upon light excitation, B-PyTT-COP in methanol displayed a continuous, strong, and broad absorption in the effectively excited state absorption (ESA) (positive signal) of the singlet excited state [85], with the absorption peak maximum observed at 860 nm. This phenomenon was attributed to the rapid trapping of electrons and slow recombination of photogenerated carriers within B-PyTT-COP (Fig. 7a). In contrast, Su-PyTT-COP exhibited a weak absorption peak at 700 nm, presented as an opposing signal (ground-state bleach), which is consistent with the high recombination for these COPs [86] (Fig. 7b). These findings were confirmed through additional investigations of B-PyTT-COP and Su-PyTT-COP under photocatalytic conditions, including the presence of a sacrificial reagent (0.1 M of AA) and co-catalyst (4 wt% of H_2PtCl_6) (Fig. 7c and Fig. S51). Additionally, kinetic decay curves of two COPs when dissolved in methanol were fitted using a three-exponential function. B-PyTT-COP demonstrated a longer decay average lifetime (τ_{avg} = 97.491 ps) while Su-PyTT-COP exhibited a lower average decay lifetime (τ_{avg} = 18.88 ps) (Fig. 7d and e). Similarly, the results showed low recombination and fast charge transfer and separation for photogenerated electrons in B-PyTT-COP (PC) with longer τ_{avg} (188.06 ps) and vice versa in the Su-PyTT-COP with smaller τ_{avg} (10.672 ps) (Fig. 7f and Fig. S51). In Fig. 7g, we present a schematic diagram illustrating the relationship between the insertion of benzoin linkage into the COPs network and photocatalytic activity based on the previous results. In the case of the Su-PyTT-COP, after photoexcitation, the electrons transfer from D to π-spacer, but the absence of the benzoin linkage reduces the delocalization of excited electrons over the COP network, leading to the recombination of photogenerated electrons from π-spacer to D. This results in a shorter bleach recovery lifetime and ineffective charge separation. On the other hand, the insertion of benzoin linkages (B-PyTT-COP) enables effective charge separation and significantly decreased charge recombination due to the introduction of a D-π-A system, which promotes delocalization between D-π-spacer of different repeated moieties and efficient charge transfer to A (benzoin linkage). This suggests that photogenerated carriers gain increased chances in the photocatalytic reaction, reducing the recombination of excited electrons and holes [87] for B-PyTT-COP. Consequently, this enhances the efficiency of carrier separation and transfer. These results strongly support the enhancement of photocatalytic hydrogen evolution upon the insertion of benzoin linkages into the COP network. Furthermore, this finding is corroborated by complementary analyses including UV–Vis DRS, band gap, PL, TCSPC, EPR, and EIS.

3.6. DFT, TD-DFT, and ESP calculations for B-PyTT-COP

The molecular orbitals of PyTT-COP could provide a comprehensive understanding of the electronic structure. Fig. 8a of HOMO-1, HOMO, LUMO, and LUMO + 1 orbitals illustrate the reactive sites and electronic transitions of the PyTT-COP, serving as key indicators of the energy levels associated with electrons within the material. The electron density is distributed over pyrene moiety in the HOMO, which moved to thiophene and benzoin moieties in LUMO at higher wavelengths of around 468 nm. The LUMO is predominantly delocalized over both the thiophene ring and the benzoin linkage. A novel hydrophilic acceptor, represented by the benzoin linkage, is introduced, thereby creating a new Donor-π-Acceptor hydrophilic system (D-π-A). This system incorporates a pyrene moiety as the donor, thiophene serving as the π-spacer, and the benzoin linkage functioning as the acceptor. In addition, LUMO + 1 assumes importance in comprehending properties associated with excited states, providing valuable insights of almost full contribution of thiophene and benzoin moieties in the excited state based on the lower wavelength of 398 nm. However, MO shows significance lies in facilitating charge transfer processes, electronic transitions, and optical properties within the molecular framework toward the HER.

The DOS plot of Fig. 8b refers to the contributions of benzoin, thiophene, and pyrene moieties and the distribution of electronic density across different energy values. In addition, the numerical molecular orbital contributions of benzoin, thiophene, and pyrene moieties at different energy levels (HOMO-1, HOMO, LUMO, LUMO + 1) gives a quantitative understanding of the electron distribution (Fig. 8c). The percentages indicate the proportion of each moiety's contribution at specific energy levels. This helps in understanding the relative importance of each component in different electronic states.

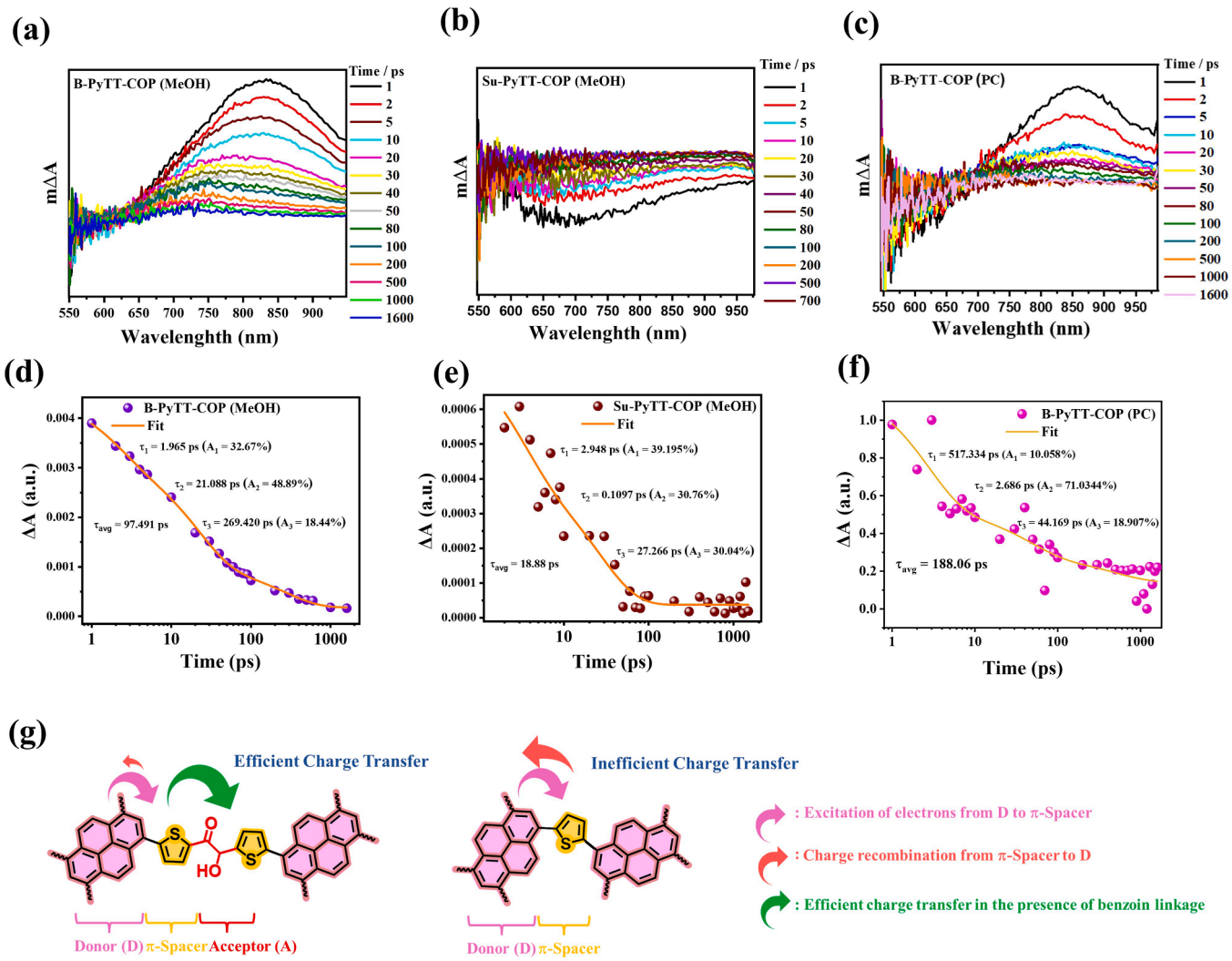

Fig. 7. fs-TA spectra at different time delays after femtosecond laser excitation at 460 nm of (a) B-PyTT-COP in methanol as a solvent, (b) Su-PyTT-COP in methanol as a solvent, (c) B-PyTT-COP in photocatalytic condition, not, PC indicates to photocatalytic condition. fs-TA decay fitting results of (d) B-PyTT-COP in methanol as a solvent at 860 nm, (e) Su-PyTT-COP in methanol as a solvent at 700 nm, (f) B-PyTT-COP in photocatalytic condition at 860 nm. Schematic diagram presenting the effect of benzoin linkage insertion on the charge transfer using D-π-A system repeated moieties of the COPs and the charge recombination between the donor and π-spacer (g).

Benzoin and thiophene moieties consistently exhibit significant contributions, particularly in lower energy orbitals of excited states, suggesting their importance of benzoin and thiophene moieties in determining the electronic properties of B-PyTT-COP toward the reduction state and intermolecular charge transfer to Pt-cocatalyst for HER. In contrast, pyrene orbitals prominence in higher energy orbitals of ground states indicates its influence on excited states and overall molecular stability.

The simulate the electronic transitions that occur during absorption of light of UV–Vis. absorption spectrum of B-PyTT-COP was performed using Time-Dependent Density Functional Theory (TD-DFT) calculations which is commonly employed to study electronic excitations in molecules. The electronic excitations of the S1 state show excitation energy is 2.65 eV, corresponding to a wavelength of 468 nm, which implies the absorption of light in the visible range. In addition, the high oscillator strength (f = 0.945) indicates a strong transition probability for this electronic excitation (Fig. 8d). This also confirms the significant transition from orbital HOMO to LUMO has a transition dipole moment of 0.699, indicating the direction and strength of the transition. In addition, a weaker transition compared to the first excited state with the excitation energy of 3.12 eV, which corresponds to slightly higher energy and a shorter wavelength of 398.0 nm due to the transition from HOMO to LUMO + 1 state. However, the electrostatic potential (ESP) mapping investigates the distribution of electron density within the B-PyTT-COP, which indicates that the high distribution of negativity charge on atoms in the thiophene and benzoin linkage suggests a significant correlation with reactivity towards the hydrogen evolution reaction (HER) (Fig. 8e).

3.7. Photocatalytic oxygen evolution reaction (OER) of COPs with and without benzoin linkage

All benzoin-based COPs (B-PyTT-COP, B-PyTP-CO, B-TFPB-COP, B-TriFPB-COP, and B-TPA-COP) exhibited suitable VBM ranging from 5.72 to 6.31 eV, indicating their potential for photocatalytic OER [70,88] (Fig. 9a, b and Fig. S38). This was further confirmed by experiments under visible light irradiation using $AgNO_3$ as a sacrificial electron acceptor (SEA) and La_2O_3 as a pH buffer. Different dosages of B-PyTT-COP investigated the highest activity reaching 244.00 μmol $g^{-1}h^{-1}$ OER of 2 mg, surpassing control experiments without a catalyst or electron acceptor (Fig. 9a and Table S4). Notably, B-PyTP-COP achieved a high OER of 471.90 μmol $g^{-1}h^{-1}$, which may be attributed to the unique

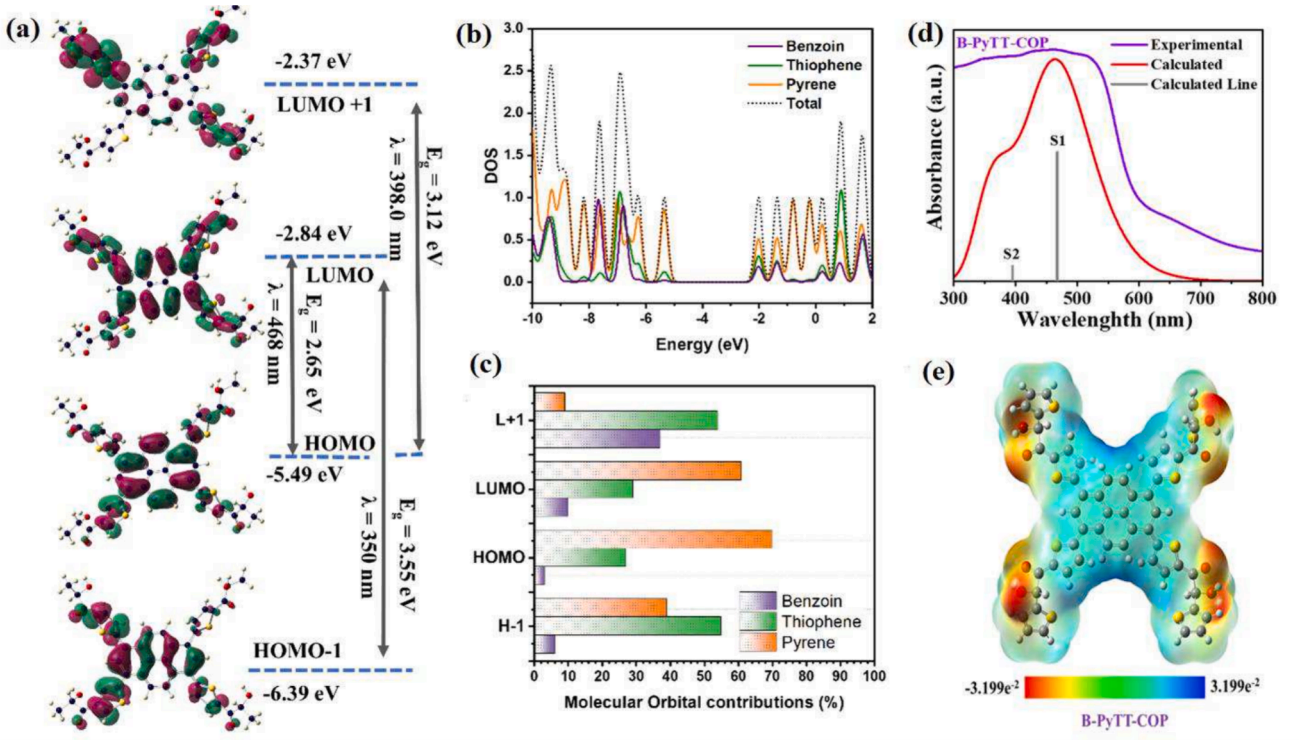

Fig. 8. DFT results (a) of PyTT-COP of MO visualization, (b) of Density of state, (d) of projected DOS. Simulated electronic transitions of B-PyTT-COP (d). Electrostatic potential mapping of B-PyTT-COP (e).

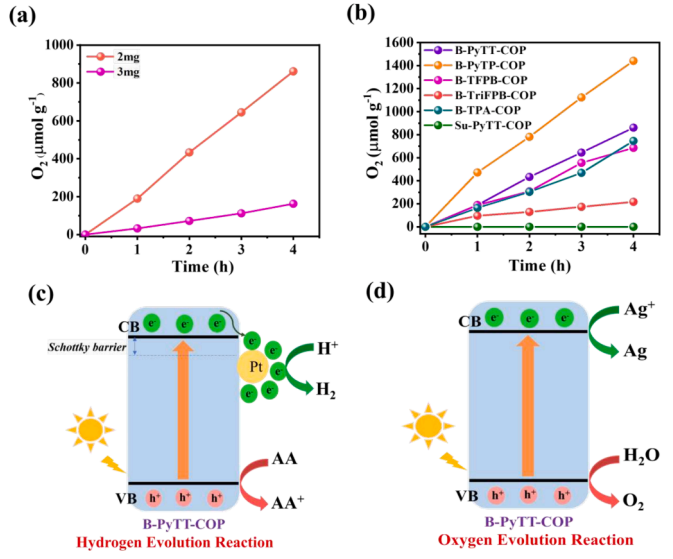

Fig. 9. Different weights of B-PyTT-COP for O_2 generation (a). O_2 evolution rate (OER) (b)of COP with and without benzoin bridge (2.0 mg) under visible light illumination in the presence of $AgNO_3$ (0.05 M, 10 mL) and La_2O_3 (15 mg). Photocatalytic plausible mechanism for B-PyTT-COP for hydrogen (c) and oxygen (d) evolution under visible light in the sacrificial donor and acceptor presence, respectively.

synergy of pyrene, benzene [89], and benzoin moieties in its structure. In contrast, Su-PyTT-COP does not have a suitable valence band for oxidizing water to oxygen. The structural stability of B-PyTP-COP was confirmed by FTIR spectroscopy, confirming its suitability for prolonged OER applications (Fig. S50). Overall, benzoin linkages unveil a promising strategy for designing efficient and robust photocatalysts for O_2 production.

Beyond its O_2 evolution efficiency, B-PyTT-COP exhibits outstanding H_2 evolution efficiency, reaching 233.81 μmol h^{-1} (77,935 mmol $g^{-1}h^{-1}$) under visible light irradiation. Visible light irradiation of Pt/B-PyTT-COP triggers charge transfer as illustrated in the schematic of Fig. 9c. This transfer is facilitated by the formation of a Schottky barrier at the Pt-B-PyTT-COP interface. The difference in work functions between Pt and the conduction band (CB) of B-PyTT-COP creates this barrier, causing the Fermi level of Pt to lie below the CB. Upon light absorption, photogenerated electrons in the CB can transfer to Pt nanoparticles due to the favorable energy gradient. This process continues until the Fermi levels of Pt and B-PyTT-COP reach equilibrium, achieving spatial separation of the photogenerated electron-hole pairs. The holes remaining on the valence band (VB) of B-PyTT-COP can then be neutralized using ascorbic acid which serves as a sacrificial electron donor in this system. Moreover, XPS analysis confirms the presence of Pt (0) in the Pt/B-PyTT-COP composite, as indicated by the Pt $4f_{7/2}$ and $4f_{5/2}$ peaks at 69.92 and 73.18 eV (Fig. S54a). This metallic state of Pt is essential for its co-catalytic function in promoting efficient hydrogen evolution, as corroborated by references [9091]. On the other hand, this photocatalyst is capable of producing oxygen when $AgNO_3$ is used as a sacrificial electron acceptor, as depicted in Fig. 9d. The XPS analysis of B-PyTT-COP after the photocatalytic reaction indicates that the majority of Ag(I) has been photocatalytically reduced to Ag(0) (Fig. S54b). This observation suggests that silver ions Ag(I) can effectively function as electron acceptors during the photocatalytic process. Overall, B-PyTT-COP can generate H_2 and O_2 separately.

Linear sweep voltammetry (LSV) was employed to investigate the photoresponse of all benzoin-based COPs. B-PyTT-COP and B-PyTP-COP exhibited a higher photocurrent response when light was applied compared to dark conditions (Figure S55). This suggests their enhanced photocatalytic activity under illumination. Additionally, B-PyTT-COP demonstrated good stability over a wide potential range (1 V to 3 V). This stability further enhances its photoresponse, particularly at 1.2 V.

4. Discussion

This work presents a green strategy using vitamin B1 as a catalyst to synthesize benzoin-based COPs, elucidating the crucial interface for photoinduced hydrogen evolution from water. The benzoin linkage acts as a novel acceptor within these networks, facilitating the creation of hydrophilic, non-conjugated materials for efficient hydrogen generation with high apparent quantum yield (AQY). Our primary aim was to address the limitations of conventional COP design, specifically the challenges associated with integrating hydrophilic groups, light-harvesting units, and achieving precise control over molecular structure to optimize photocatalytic activity.

Previous research by our group demonstrated the potential of non-conjugated polymers for achieving efficient hydrogen evolution [26,50,92]. While conjugated polymers excel at light absorption and charge separation, they often suffer from poor water interaction [2]. Conversely, hydrophilic non-conjugated polymers exhibit good water interaction but limited light absorption and charge separation. Integrating these contrasting functionalities could pave the way for photocatalysts with superior light absorption and water interaction.

As a proof-of-concept, we synthesized COP via Suzuki coupling (Su-PyTT-COP), representing an amorphous conjugated system (D-π). In contrast to B-PyTT-COP, this COP displayed hydrophobic characteristics, resulting in low HER, minimal AQY, and no observed OER activity. This finding highlights the benefit of switching from a conjugated to a non-continuous conjugated system, as it increases the number of active sites on the COP skeleton, facilitating faster electron transport from the skeleton to the reaction center and significantly enhancing photocatalytic efficiency (Fig. S52).

The COP skeletons based on benzoin were strategically designed for efficient hydrogen production and visible light response. Structural modifications play a critical role in photocatalytic reactions. We investigated the optimal integration of various donors and π-spacers with the benzoin bridge in benzoin-based COPs to achieve the most effective design for high photocatalytic activity. Notably, the B-PyTT-COP skeleton, featuring pyrene as a donor, thiophene as a p-spacer, and a benzoin linkage as an acceptor to form a new D-π-A system, demonstrated superior hydrogen production and light response. This COP achieved an outstanding hydrogen evolution rate of 238.81 μmol h^{-1} and a record-breaking apparent quantum efficiency (AQY) of 60.03 %, 61.10 %, and 65.35 % at 420, 460, and 500 nm, respectively, using platinum as a co-catalyst. To our knowledge, these represent the highest reported values for COP photocatalysts. Remarkably, the B-PyTT-COP exhibits an exceptional ability to generate a high AQY value at 500 nm (65.35 %), surpassing all other investigated materials to date (Fig. 5g). fs-TA and TD-DFT analyses revealed intrinsically lower exciton binding energies and longer-lived charge carriers in benzoin-based COPs compared to their counterparts without benzoin bridges. Interestingly, all synthesized benzoin-based COPs displayed OER activity, unlike those lacking the benzoin unit. Additionally, B-PyTT-COP has been successfully employed in thin-film hydrogen production techniques. This study demonstrates the universal applicability of benzoin-based COPs for significantly enhancing photocatalytic activity and apparent quantum yield.

5. Conclusion

We synthesized a series of five hydrophilic D-π-A benzoin-based COPs by reaction of multiformly monomers in the presence of Vitamin B1 with 100 % yield. Accordingly, the resulting D–π–A benzoin-based COPs exhibit high hydrophilicity, a semicrystalline network, and efficient charge transfer, resulting in excellent photocatalytic hydrogen evolution. The HER for these COPs photocatalysts increased when the pyrene moiety (donor), thiophene (π-spacer), and benzoin-linkage (novel acceptor) were integrated. This demonstrates the significant influence of the donor-π-spacer-acceptor sequence on the photocatalytic activity. As a result, B-PyTT-COP (D-π-A) showed an outstanding HER of 233.81 μmol h^{-1} (77,935.10 μmol $g^{-1}h^{-1}$) in the presence of AA as SED and 4 wt% of H_2PtCl_6 as co-catalyst and an unprecedented AQY of 60.03 %, 61.10 %, and 65.35 %, respectively, at 420, 460, and 500 nm. Remarkably, this COPs has attained an AQY value of 65.35 percent at 500 nm, exceeding all other materials that have been examined. According to TD-DFT analysis and charge carrier kinetics, benzoin-based COPs have lower exciton binding energies and longer-lived charge carriers than COPs without benzoin bridges. All benzoin-based COPs produce O_2 using silver nitrate as SAE. Thin-film technology can also be used to generate H_2 with B-PyTT-COP (D-π-A). This work reports the synthesis of a series of high hydrophilicity based-benzoin COPs using a green synthetic approach and demonstrates that these COPs can be used to boost photocatalytic activity and apparent quantum yield by varying the donor-π-spacer in the presence of benzoin linkage as acceptor.

CRediT authorship contribution statement

Islam M.A. Mekhemer: Writing – review & editing, Writing – original draft, Validation, Methodology, Formal analysis, Data curation, Conceptualization. **Ahmed M. Elewa:** Visualization, Methodology, Conceptualization. **Mohamed M. Elsenety:** Visualization, Software, Investigation. **Maha Mohamed Samy:** Methodology, Investigation, Formal analysis. **Mohamed Gamal Mohamed:** Methodology, Investigation, Formal analysis. **Ahmed Fouad Musa:** Methodology, Investigation. **Tse-Fu Huang:** Visualization, Investigation. **Tzu-Chien Wei:** Methodology, Investigation. **Shiao-Wei Kuo:** Methodology, Investigation. **Bo-Han Chen:** Investigation. **Shang-Da Yang:** Investigation. **Ho-Hsiu Chou:** Writing – review & editing, Supervision, Resources, Project administration, Funding acquisition, Conceptualization.

Declaration of competing interest

The authors declare that they have no known competing financial interests or personal relationships that could have appeared to influence the work reported in this paper.

Data availability

Data will be made available on request.

Acknowledgments

It is with great gratitude that the authors acknowledge the financial support of the National Science and Technology Council of Taiwan (NSTC 112-2221-E-007 -081 -; NSTC 112-2223-E-007 -006 -MY3; NSTC 112-2622-E-007 -032 -; NSTC 113-2923-E-007 -007 -MY3; NSTC 113-2823-8-007 -003 -) as well as the computing time provided by the National Center for High-Performance Computing of Taiwan. The authors thank the Precision Instrument Support Center of National Tsing Hua University for providing measurement and analysis facilities.

Appendix A. Supplementary data

Supplementary data to this article can be found online at https://doi.org/10.1016/j.cej.2024.154280.

References

[1] D.G. Wang, T. Qiu, W. Guo, Z. Liang, H. Tabassum, D. Xia, R. Zou, Covalent organic framework-based materials for energy applications, Energy Environ. Sci. 14 (2021) 688–728.
[2] C. Zhao, Z. Chen, R. Shi, X. Yang, T. Zhang, Recent advances in conjugated polymers for visible-light-driven water splitting, Adv. Mater. 32 (2020) 1907296.
[3] X. Wang, L. Chen, S.Y. Chong, M.A. Little, Y. Wu, W.-H. Zhu, R. Clowes, Y. Yan, M. A. Zwijnenburg, R.S. Sprick, Sulfone-containing covalent organic frameworks for photocatalytic hydrogen evolution from water, Nat. Chem. 10 (2018) 1180–1189.

[4] C. Li, J. Liu, H. Li, K. Wu, J. Wang, Q. Yang, Covalent organic frameworks with high quantum efficiency in sacrificial photocatalytic hydrogen evolution, Nat. Commun. 13 (2022) 2375.
[5] H.O. Badr, V. Natu, F. Ștefan Neațu, A. Neațu, A.M. Kuncser, M. Rostas, M. W. Racey, M Florea Barsoum, Photo-stable, 1D-nanofilaments TiO_2-based lepidocrocite for photocatalytic hydrogen production in water-methanol mixtures, Matter 6 (2023) 2853–2869.
[6] G. Liao, C. Li, B. Fang, Donor-acceptor organic semiconductor heterojunction nanoparticles for efficient photocatalytic H_2 evolution, Matter 5 (2022) 1635–1637.
[7] Q. Li, J. Li, W. Wang, L. Liu, Z. Xu, G. Xie, J. Li, J. Yao, W. Li, Tuning acceptor length in photocatalytic donor-acceptor conjugated polymers for efficient solar-to-hydrogen energy conversion, Chinese J. Chem. 40 (2022) 2457–2467.
[8] C. Han, S. Xiang, S. Jin, L.W. Luo, C. Zhang, C. Yan, J.X. Jiang, Linear multiple-thiophene-containing conjugated polymer photocatalysts with narrow band gaps for achieving ultrahigh photocatalytic hydrogen evolution activity under visible light, J. Mater. Chem. A 10 (2022) 5255–5261.
[9] Q. Li, K.-H. Li, L.-N. Liu, Z.-X. Xue, Z.-W. Xu, W.-S. Li, Conjugated polyelectrolyte photocatalysts: the use of zwitterionic side groups for high performance, ACS Appl. Polym. Mater. 5 (2023) 8570–8578.
[10] M.Z. Rahman, J. Gascon, Determining the sequence of charge transport events and their roles on the limit of quantum efficiency of photocatalytic hydrogen production, Matter 6 (2023) 2081–2093.
[11] W. Zhang, Y. Liu, G. Yu, Heteroatom substituted organic/polymeric semiconductors and their applications in field-effect transistors, Adv. Mater. 26 (2014) 6898–6904.
[12] Y. Takeda, T.L. Andrew, J.M. Lobez, A.J. Mork, T.M. Swager, An air-stable low-bandgap n-type organic polymer semiconductor exhibiting selective solubility in perfluorinated solvents, Angew Chemie 124 (2012) 9176–9180.
[13] Z. Zhang, J. Jia, Y. Zhi, S. Ma, X. Liu, Porous organic polymers for light-driven organic transformations, Chem. Soc. Rev. 51 (2022) 2444–2490.
[14] M.V. Pavliuk, S. Wrede, A. Liu, A. Brnovic, S. Wang, M. Axelsson, H. Tian, Preparation, characterization, evaluation and mechanistic study of organic polymer nano photocatalysts for solar fuel production, Chem. Soc. Rev. 51 (2022) 6909–6935.
[15] Y. Li, M. Karimi, Y.N. Gong, N. Dai, V. Safarifard, H.L. Jiang, Integration of metal-organic frameworks and covalent organic frameworks: design, synthesis, and applications, Matter 4 (2021) 2230–2265.
[16] Y. Qin, P. She, Y. Wang, W. Wong, An all-in-one integrating strategy for designing platinum (II)-based supramolecular polymers for photocatalytic hydrogen evolution, Small 2400259 (2024).
[17] I.M.A. Mekhemer, Y. Wu, A.M. Elewa, W. Chen, C. Chueh, H. Chou, Naphthalenediimide-based polymer dots with dual acceptors as a new class of photocatalysts for photocatalytic hydrogen generation under visible light irradiation, Sol. RRL (2024) 2300994.
[18] L. Wang, L. Liu, Y. Li, Y. Xu, W. Nie, Z. Cheng, Q. Zhou, L. Wang, Z. Fan, Molecular-level regulation strategies toward efficient charge separation in donor− acceptor type conjugated polymers for boosted energy-related photocatalysis, Adv. Energy Mater. 14 (2024) 2303346.
[19] M.H. Elsayed, M. Abdellah, A.Z. Alhakemy, I.M.A. Mekhemer, A.E.A. Aboubakr, B. H. Chen, A. Sabbah, K.H. Lin, W.S. Chiu, S.J. Lin, Overcoming small-bandgap charge recombination in visible and NIR-light-driven hydrogen evolution by engineering the polymer photocatalyst structure, Nat. Commun. 15 (2024) 707.
[20] I.M.A. Mekhemer, M. Elsenety, A. Elewa, K.D.G. Huynh, M.M. Samy, M. G. Mohamed, D.M. Dorrah, D.C.K. Hoang, A.F. Musa, S.W. Kuo, H.H. Chou, Push-pull-pull interactions of 2D imide-imine based covalent organic framework to promote charge separation in photocatalytic hydrogen production, J. Mater. Chem. a. 12 (2024) 10790–10798.
[21] Q. Yang, P. Peng, Z. Xiang, Covalent organic polymer modified TiO_2 nanosheets as highly efficient photocatalysts for hydrogen generation, Chem. Eng. Sci. 162 (2017) 33–40.
[22] A. Thomas, Functional materials: from hard to soft porous frameworks, Angew. Chemie Int. Ed. 49 (2010) 8328–8344.
[23] N. Du, H.B. Park, G.P. Robertson, M.M. Dal-Cin, T. Visser, L. Scoles, M.D. Guiver, Polymer nanosieve membranes for CO_2-capture applications, Nat. Mater. 10 (2011) 372–375.
[24] O.M. Yaghi, M. O'Keeffe, N.W. Ockwig, H.K. Chae, M. Eddaoudi, J. Kim, Reticular synthesis and the design of new materials, Nature 423 (2003) 705–714.
[25] H.A. Patel, S. Hyun Je, J. Park, D.P. Chen, Y. Jung, C.T. Yavuz, A. Coskun, Unprecedented high-temperature CO_2 selectivity in N_2-phobic nanoporous covalent organic polymers, Nat. Commun. 4 (2013) 1–8.
[26] A.M. Elewa, M.H. Elsayed, A.F.M. El-Mahdy, C.L. Chang, L.Y. Ting, W.C. Lin, C. Y. Lu, H.H. Chou, Triptycene-based discontinuously-conjugated covalent organic polymer photocatalysts for visible-light-driven hydrogen evolution from water, Appl. Catal. B Environ. 285 (2021) 119802.
[27] Z. Miao, G. Liu, Y. Cui, Z. Liu, J. Li, F. Han, Y. Liu, X. Sun, X. Gong, Y. Zhai, A novel strategy for the construction of covalent organic frameworks from nonporous covalent organic polymers, Angew Chemie 131 (2019) 4960–4964.
[28] T. Skorjanc, D. Shetty, M. Valant, Covalent organic polymers and frameworks for fluorescence-based sensors, ACS Sensors 6 (2021) 1461–1481.
[29] Z. Xiang, X. Zhou, C. Zhou, S. Zhong, X. He, C. Qin, D. Cao, Covalent-organic polymers for carbon dioxide capture, J. Mater. Chem. 22 (2012) 22663–22669.
[30] A. Mukhtar, S. Saqib, N.B. Mellon, M. Babar, S. Rafiq, S. Ullah, M.A. Bustam, A. G. Al-Sehemi, N. Muhammad, M. Chawla, CO_2 capturing, thermo-kinetic principles, synthesis and amine functionalization of covalent organic polymers for CO_2 separation from natural gas: a review, J. Nat. Gas Sci. Eng. 77 (2020) 103203.
[31] D. Yadav, S.K. Awasthi, A Pd NP-confined novel covalent organic polymer for catalytic applications, New J. Chem. 44 (2020) 1320–1325.
[32] K. Prakash, K. Chaudhary, D.T. Masram, A new triazine-cored covalent organic polymer for catalytic applications, Appl. Catal. A Gen. 593 (2020) 117411.
[33] A. Hassan, A. Alam, M. Ansari, N. Das, Hydroxy functionalized triptycene based covalent organic polymers for ultra-high radioactive iodine uptake, Chem. Eng. J. 427 (2022) 130950.
[34] F. Alduraiei, S. Kumar, J. Liu, S.P. Nunes, G. Szekely, Rapid fabrication of fluorinated covalent organic polymer membranes for organic solvent nanofiltration, J. Memb. Sci. 648 (2022) 120345.
[35] M.C. Scicluna, L. Vella-Zarb, Evolution of nanocarrier drug-delivery systems and recent advancements in covalent organic framework–drug systems, ACS Appl. Nano Mater. 3 (2020) 3097–3115.
[36] X. Feng, L. Liu, Y. Honsho, A. Saeki, S. Seki, S. Irle, Y. Dong, A. Nagai, D. Jiang, High-rate charge-carrier transport in porphyrin covalent organic frameworks: switching from hole to electron to ambipolar conduction, Angew Chemie 124 (2012) 2672–2676.
[37] N. Nouruzi, M. Dinari, B. Gholipour, N. Mokhtari, M. Farajzadeh, S. Rostamnia, M. Shokouhimehr, Photocatalytic hydrogen generation using colloidal covalent organic polymers decorated bimetallic Au-Pd nanoalloy (COPs/Pd-Au), Mol. Catal. 518 (2022) 112058.
[38] Y. Liu, Z. Xiang, Fully conjugated covalent organic polymer with carbon-encapsulated Ni_2P for highly sustained photocatalytic H_2 production from seawater, ACS Appl. Mater. Interfaces 11 (2019) 41313–41320.
[39] Y. Liu, Z. Liao, X. Ma, Z. Xiang, Ultrastable and efficient visible-light-driven hydrogen production based on donor–acceptor copolymerized covalent organic polymer, ACS Appl. Mater. Interfaces 10 (2018) 30698–30705.
[40] J. Chen, X. Tao, L. Tao, H. Li, C. Li, X. Wang, C. Li, R. Li, Q. Yang, Novel conjugated organic polymers as candidates for visible-light-driven photocatalytic hydrogen production, Appl. Catal. B Environ. 241 (2019) 461–470.
[41] C. Dai, Y. Pan, B. Liu, Conjugated polymer nanomaterials for solar water splitting, Adv. Energy Mater. 10 (2020) 2002474.
[42] T. Banerjee, F. Podjaski, J. Kröger, B.P. Biswal, B.V. Lotsch, Polymer photocatalysts for solar-to-chemical energy conversion, Nat. Rev. Mater. 6 (2021) 168–190.
[43] Y. Sun, V. Kumar, K.H. Kim, The assessment of graphitic carbon nitride ($g\text{-}C_3N_4$) materials for hydrogen evolution reaction: effect of metallic and non-metallic modifications, Sep. Purif. Technol. 122413 (2022).
[44] W.J. Xiao, Y. Wang, W.R. Wang, J. Li, J. Wang, Z.W. Xu, J. Li, J. Yao, W.S. Li, Diketopyrrolopyrrole-based donor–acceptor conjugated microporous polymers for visible-light-driven photocatalytic hydrogen production from water, Macromolecules 53 (2020) 2454–2463.
[45] Z. Xiang, Q. Dai, J. Chen, L. Dai, Edge functionalization of graphene and two-dimensional covalent organic polymers for energy conversion and storage, Adv. Mater. 28 (2016) 6253–6261.
[46] Y. Liu, J. Wu, F. Wang, Dibenzothiophene-S, S-dioxide-containing conjugated polymer with hydrogen evolution rate up to 147 mmol/g $^{h-}$1, Appl. Catal. B Environ. 307 (2022) 121144.
[47] W.-C. Lin, J. Jayakumar, C.-L. Chang, L.-Y. Ting, T.-F. Huang, M.H. Elsayed, A. M. Elewa, Y.-T. Lin, J.-J. Liu, Y.-T. Tseng, Sulfide oxidation tuning in 4, 8-bis (5-(2-ethylhexyl) thiophen-2-yl) benzo [1, 2-b: 4, 5-b′] dithiophene based dual acceptor copolymers for highly efficient photocatalytic hydrogen evolution, J. Mater. Chem. A 10 (2022) 6641–6648.
[48] C. Shu, C. Han, X. Yang, C. Zhang, Y. Chen, S. Ren, F. Wang, F. Huang, J. Jiang, Boosting the photocatalytic hydrogen evolution activity for D–π–A conjugated microporous polymers by statistical copolymerization, Adv. Mater. 33 (2021) 2008498.
[49] S.B. Yu, F. Lin, J. Tian, J. Yu, D.W. Zhang, Z.T. Li, Water-soluble and dispersible porous organic polymers: preparation, functions and applications, Chem. Soc. Rev. 51 (2022) 434–449.
[50] C.L. Chang, W.C. Lin, L.Y. Ting, C.H. Shih, S.Y. Chen, T.F. Huang, H. Tateno, J. Jayakumar, W.Y. Jao, C.W. Tai, Main-chain engineering of polymer photocatalysts with hydrophilic non-conjugated segments for visible-light-driven hydrogen evolution, Nat. Commun. 13 (2022) 5460.
[51] R. Li, X. Zhang, T. Wang, C. Li, L. Luo, C.-X. Cui, W. Zhang, J.-C. Wang, H. Tang, R. Zhang, Delicately regulating the π-spacer of D− π–A-conjugated polymers for improved visible-light-driven hydrogen evolution, Macromolecules 57 (2024) 2057–2066.
[52] J. Yang, X. Zhang, W. Si, Y. Cao, J. Qian, Y. Li, B. Li, W. Qin, Alkene-bridged ionic covalent organic nanosheets (iCONs) based on D-π-A for photocatalytic hydrogen evolution, ACS Catal. 14 (2024) 2022–2030.
[53] Y. Deng, Y. Shi, L. Li, R. Tang, Z. Zhou, S. Xiong, W. Li, J. Liu, Y. Huang, Molecular modification: a promising strategy for the design of donor-acceptor-type organic polymers photocatalyst, Appl. Catal. B Environ. Energy (2024) 124043.
[54] L. Li, Z. Cai, Q. Wu, W.-Y. Lo, N. Zhang, L.X. Chen, L. Yu, Rational design of porous conjugated polymers and roles of residual palladium for photocatalytic hydrogen production, J. Am. Chem. Soc. 138 (2016) 7681–7686.
[55] C. Han, P. Dong, H. Tang, P. Zheng, C. Zhang, F. Wang, F. Huang, J.-X. Jiang, Realizing high hydrogen evolution activity under visible light using narrow band gap organic photocatalysts, Chem. Sci. 12 (2021) 1796–1802.
[56] C. Han, S. Xiang, S. Jin, C. Zhang, J.-X. Jiang, Rational design of conjugated microporous polymer photocatalysts with definite D−π–A structures for ultrahigh photocatalytic hydrogen evolution activity under natural sunlight, ACS Catal. 13 (2022) 204–212.
[57] C. Han, S. Xiang, P. Xie, P. Dong, C. Shu, C. Zhang, J. Jiang, A universal strategy for boosting hydrogen evolution activity of polymer photocatalysts under visible light

by inserting a narrow-band-gap spacer between donor and acceptor, Adv. Funct. Mater. 32 (2022) 2109423.
[58] R.H. Friend, R.W. Gymer, A.B. Holmes, J.H. Burroughes, R.N. Marks, C. Taliani, D. D.C. Bradley, D.A. Dos Santos, J.-L. Bredas, M. Lögdlund, Electroluminescence in conjugated polymers, Nature 397 (1999) 121–128.
[59] Y. Bai, C. Li, L. Liu, Y. Yamaguchi, M. Bahri, H. Yang, A. Gardner, M. A. Zwijnenburg, N.D. Browning, A.J. Cowan, Photocatalytic overall water splitting under visible light enabled by a particulate conjugated polymer loaded with palladium and iridium, Angew. Chemie 134 (2022) e202201299.
[60] D. Kieslich, J. Christoffers, Cyanide anions as nucleophilic catalysts in organic synthesis, Synthesis (stuttg). 53 (2021) 3485–3496.
[61] M.A. Abd-Alla, Novel synthesis of poly (benzoin) and poly (benzil). Characterization and application as photosensitizer materials, Die Makromol, Chemie 192 (1991) 277–283.
[62] M. Alrayyani, O.Š. Miljanić, Benzoins and cyclobenzoins in supramolecular and polymer chemistry, Chem. Commun. 54 (2018) 11989–11997.
[63] Y.C. Zhao, T. Wang, L.-M. Zhang, Y. Cui, B.-H. Han, Facile approach to preparing microporous organic polymers through benzoin condensation, ACS Appl. Mater. Interfaces 4 (2012) 6975–6981.
[64] J.P. Morgan, E.E. Torres, R. Averill, A.M. Brody, Updating the benzoin condensation of benzaldehyde using microwave-assisted organic synthesis and N-heterocyclic carbene catalysis, J. Chem. Educ. 100 (2023) 986–990.
[65] V. Sublett, Synthesis of Dilantin Using the Principles of Green Chemistry, (2017).
[66] L. Baragwanath, C.A. Rose, K. Zeitler, S.J. Connon, Highly enantioselective benzoin condensation reactions involving a bifunctional protic pentafluorophenyl-substituted triazolium precatalyst, J. Org. Chem. 74 (2009) 9214–9217.
[67] X. Gao, C. Shu, C. Zhang, W. Ma, S.-B. Ren, F. Wang, Y. Chen, J.H. Zeng, J.-X. Jiang, Substituent effect of conjugated microporous polymers on the photocatalytic hydrogen evolution activity, J. Mater. Chem. A 8 (2020) 2404–2411.
[68] T.P. Le, B.H. Smith, Y. Lee, J.H. Litofsky, M.P. Aplan, B. Kuei, C. Zhu, C. Wang, A. Hexemer, E.D. Gomez, Enhancing optoelectronic properties of conjugated block copolymers through crystallization of both blocks, Macromolecules 53 (2020) 1967–1976.
[69] C.P. Chen, S.-H. Chan, T.-C. Chao, C. Ting, B.-T. Ko, Low-bandgap poly (thiophene-phenylene-thiophene) derivatives with broaden absorption spectra for use in high-performance bulk-heterojunction polymer solar cells, J. Am. Chem. Soc. 130 (2008) 12828–12833.
[70] W. Li, X. Huang, T. Zeng, Y.A. Liu, W. Hu, H. Yang, Y. Zhang, K. Wen, Thiazolo [5, 4-d] thiazole-based donor-acceptor covalent organic framework for sunlight-driven hydrogen evolution, Angew Chemie 133 (2021) 1897–1902.
[71] S. Kandambeth, A. Mallick, B. Lukose, M.V. Mane, T. Heine, R. Banerjee, Construction of crystalline 2D covalent organic frameworks with remarkable chemical (acid/base) stability via a combined reversible and irreversible route, J. Am. Chem. Soc. 134 (2012) 19524–19527.
[72] S. Cao, J. Yu, Carbon-based H_2-production photocatalytic materials, J. Photochem. Photobiol. C Photochem. Rev. 27 (2016) 72–99.
[73] M.M. Samy, I.M.A. Mekhemer, M.G. Mohamed, M.H. Elsayed, K.-H. Lin, Y.-K. Chen, T.-L. Wu, H.-H. Chou, S.-W. Kuo, Conjugated Microporous Polymers Incorporating Thiazolo [5, 4-d] thiazole Moieties for Sunlight-Driven Hydrogen Production From Water, Chem. Eng. J. 137158 (2022).
[74] Y. Wang, W. Hao, H. Liu, R. Chen, Q. Pan, Z. Li, Y. Zhao, Facile construction of fully sp2-carbon conjugated two-dimensional covalent organic frameworks containing benzobisthiazole units, Nat. Commun. 13 (2022) 1–7.
[75] J. Zhuang, D. Tang, W. Lai, M. Xu, D. Tang, Target-induced nano-enzyme reactor mediated hole-trapping for high-throughput immunoassay based on a split-type photoelectrochemical detection strategy, Anal. Chem. 87 (2015) 9473–9480.
[76] M. Qureshi, K. Takanabe, Insights on measuring and reporting heterogeneous photocatalysis: efficiency definitions and setup examples, Chem. Mater. 29 (2017) 158–167.
[77] M. Rahman, H. Tian, T. Edvinsson, Revisiting the limiting factors for overall water-splitting on organic photocatalysts, Angew Chemie 132 (2020) 16418–16433.
[78] W.T. Chung, I.M.A. Mekhemer, M.G. Mohamed, A.M. Elewa, A.F.M. EL-Mahdy, H.-H. Chou, S.-W. Kuo, K.C.-W. Wu, Recent advances in metal/covalent organic frameworks based materials: their synthesis, structure design and potential applications for hydrogen production, Coord. Chem. Rev. 483 (2023) 215066.
[79] Y. Gogotsi, R.M. Penner, Energy storage in nanomaterials–capacitive, pseudocapacitive, or battery-like? ACS Nano 12 (2018) 2081–2083.
[80] E.J. Luber, J.M. Buriak, Reporting performance in organic photovoltaic devices, ACS Nano 7 (2013) 4708–4714.
[81] S. Cao, L. Piao, Considerations for a more accurate evaluation method for photocatalytic water splitting, Angew. Chemie Int. Ed. 59 (2020) 18312–18320.
[82] T.A. Kandiel, R. Dillert, L. Robben, D.W. Bahnemann, Photonic efficiency and mechanism of photocatalytic molecular hydrogen production over platinized titanium dioxide from aqueous methanol solutions, Catal. Today 161 (2011) 196–201.
[83] N. Alenzi, W.S. Liao, P.S. Cremer, V. Sanchez-Torres, T.K. Wood, C. Ehlig-Economides, Z. Cheng, Photoelectrochemical hydrogen production from water/methanol decomposition using Ag/TiO_2 nanocomposite thin films, Int. J. Hydrogen Energy 35 (2010) 11768–11775.
[84] B. Yoo, K.-J. Kim, S.-Y. Bang, M.J. Ko, K. Kim, N.-G. Park, Chemically deposited blocking layers on FTO substrates: effect of precursor concentration on photovoltaic performance of dye-sensitized solar cells, J. Electroanal. Chem. 638 (2010) 161–166.
[85] E. Nikoloudakis, M. Pigiaki, M.N. Polychronaki, A. Margaritopoulou, G. Charalambidis, E. Serpetzoglou, A. Mitraki, P.A. Loukakos, A.G. Coutsolelos, ACS Sustainable Chem, Eng 9 (2021) 7781–7791.
[86] X. Ruan, C. Huang, H. Cheng, Z. Zhang, Y. Cui, Z. Li, T. Xie, K. Ba, H. Zhang, L. Zhang, A twin S-scheme artificial photosynthetic system with self-assembled heterojunctions yields superior photocatalytic hydrogen evolution rate, Adv. Mater. 35 (2023) 2209141.
[87] A.A. Cordones, C. Das Pemmaraju, J.H. Lee, I. Zegkinoglou, M.-E. Ragoussi, F. J. Himpsel, G. de la Torre, R.W. Schoenlein, Excited-state charge distribution of a donor– π–acceptor Zn porphyrin probed by N K-Edge transient absorption spectroscopy, J. Phys. Chem. Lett. 12 (2021) 1182–1188.
[88] Y. Chen, J. Jayakumar, C. Hsieh, T. Wu, C. Liao, J. Pandidurai, C. Ko, W. Hung, C. Cheng, Triarylamine-pyridine-carbonitriles for organic light-emitting devices with EQE nearly 40%, Adv. Mater. 33 (2021) 2008032.
[89] Y. Zhang, Z. Qiao, R. Zhang, Z. Wang, H. Wang, J. Zhao, D. Cao, S. Wang, Multicomponent synthesis of imidazole-linked fully conjugated 3D Covalent organic framework for efficient electrochemical hydrogen peroxide production, Angew. Chemie 135 (2023) e202314539.
[90] N. Cao, L. Yang, H. Dai, T. Liu, J. Su, X. Wu, W. Luo, G. Cheng, Immobilization of ultrafine bimetallic Ni–Pt nanoparticles inside the pores of metal–organic frameworks as efficient catalysts for dehydrogenation of alkaline solution of hydrazine, Inorg. Chem. 53 (2014) 10122–10128.
[91] Z. Liu, X. Lin, J.Y. Lee, W. Zhang, M. Han, L.M. Gan, Preparation and characterization of platinum-based electrocatalysts on multiwalled carbon nanotubes for proton exchange membrane fuel cells, Langmuir 18 (2002) 4054–4060.
[92] C. Chang, T. Huang, W. Lin, L. Ting, C. Shih, Y. Chen, J. Liu, Y. Lin, Y. Tseng, Y. Wu, Synergistic Effect of Crown Ether and Main-Chain Engineering for Boosting Hydrogen Evolution of Polymer Photocatalysts in Seawater, Adv. Energy Mater. (n. d.) 2300986.